Development of an EMAT In-Line Inspection System For Detection, Discrimination, and Grading of Stress Corrosion Cracking In Pipelines

Annual Technical Progress Report

Reporting Period Start Date: 10/1/2001

Reporting Period End Date: 1/31/203

Principal Authors:

Jeff Aron, Jon Gore, Roger Dalton, Stuart Eaton, Adrian Bowles, Owen Thomas, Tim Jarman

Issue Date: July 2003

DOE Award Number: DE-FC26-01NT41154

Submitted by:

Contractor
Tuboscope Pipeline Services
2835 Holmes Road
Houston, TX 77051

Subcontractor
QinetiQ ltd.
Cody Technology Park
Ively Road, Farnborough
Hants GU14 0LX UK

DOE Project Officer:
Daniel Driscoll
US Department of Energy National Energy Technology Laboratory (NETL)

Disclaimer:

"This report was prepared as an account of work sponsored by an agency of the United States Government. Neither the United States Government nor any agency thereof, nor any of their employees, makes any warranty, express or implied, or assumes any legal liability or responsibility for the accuracy, completeness, or usefulness of any information, apparatus, product, or process disclosed, or represents that its use would not infringe privately owned rights. Reference herein to any specific commercial product, process, or service by trade name, trademark, manufacturer, or otherwise does not necessarily constitute or imply its endorsement, recommendation, or favoring by the United States Government or any agency thereof. The views and opinions of authors expressed herein do not necessarily state or reflect those of the United States Government or any agency thereof**. "**

Abstract:

This report describes progress, experiments, and results for a project to develop a pipeline in-line inspection tool that uses electromagnetic acoustic transducers (EMATs) to detect and grade stress corrosion cracking (SCC). There is a brief introduction that gives background material about EMATs and relevant previous Tuboscope work toward a tool. This work left various choices about the modes and transducers for this project.

The experimental section then describes the lab systems, improvements to these systems, and setups and techniques to narrow the choices. Improvements, which involved transducer matching networks, better magnetic biasing, and lower noise electronics, led to improved signal to noise (SNR) levels. The setups permitted transducer characterizations and interaction measurements in plates with man-made cracks, pipeline sections with SCC, and a full pipe with SCC. The latter were done with a moveable and compact EMAT setup, called a lab mouse, which is detailed.

Next, the results section justifies the mode and transducer choices. These were for magnetostrictive EMATs and the use of EMAT launched modes: SH0 (at 2.1 MHz-mm) and SV1 (at 3.9 MHz-mm). This section then gives details of measurements on these modes. The measurements consisted of signal to noise ratio, insertion loss, magnetic biasing sensitivities crack reflection and transmission coefficients, beam width, standoff and tilt sensitivities. For most of the measurements the section presents analysis curves, such as reflection coefficient versus crack depth. Some notable results for the chosen modes are: that acceptable SNRs were generated in a pipe with magnetostrictive EMATs, that optimum bias for magnetostrictive transmitters and receivers is magnetic saturation, that crack reflection and transmission coefficients from crack interactions agree with 2 D simulations and seem workable for crack grading, and that the mouse has good waveform quality and so is ready for exhaustive measurement EMAT scans of SCC interactions. This section also reviews further coil optimisation and implementation requirements. These involve transmitter and receiver power, acquisition parameters, and magnetic configuration. At this time all these seem reasonable for an ILI tool.

TABLE OF CONTENTS

Introduction

In recent years, concern has grown in the pipeline industry about stress-corrosion cracking (SCC), a complex phenomenon where colonies of tiny cracks form on steel pipe surfaces. Stress Corrosion Cracking [1] is a significant issue if not detected, under certain conditions the cracks can grow over a period of years and eventually lead to pipeline rupture. Consequently, it is important to detect SCC as early as possible, grade it, and monitor its growth to prevent pipeline failures. SCC presents various challenges because the cracks are very narrow and axially oriented and occurs in gas lines, so that conventional magnetic and liquid coupled ultrasonics do not work well.

An EMAT Electromagnetic Acoustic Transducer [2, 3] based system is a possible means to monitor SCC. In this technique, coils and permanent magnets are located in close proximity to, but not in contact with the external surface of the material. The coils are excited with radio frequency (RF) current and create high frequency eddy currents or magnetic fields in the material. These interact with a static magnetic bias and produce mechanical strains in the material and hence give rise to ultrasonic waves. The waves can be used for detecting and measuring defects, cracks and flaws by transmission and reflection analyses [4, 5].

By way of review there are two basic types of EMATs: magnetostrictive [6, 7] and Lorentz [2,3, 8]. These are diagrammed in Figures 1 and 2. A magnetostrictive EMAT uses the fact that pipe materials undergo magnetostriction, which means that is they stretch under a magnetic field and shrink to normal size when that field is removed. The coil creates a high frequency magnetic field in the pipe wall, which in turn creates waves by the stretching and shrinking. In a magnetostrictive EMAT the magnetic bias field linearizes, strengthens, and directs the strain effects. This field is in the plane of the pipe wall, and the bias magnets can be separated from the RF coil. In a Lorentz EMAT, the coil creates eddy currents in the wall, which then create forces in the wall via Lorentz interaction with the bias field. In the Lorentz EMAT, the bias field is perpendicular to the pipe wall, and the magnet must be over the coil.

The ultrasonic energy of interest for cracks that EMATs excite consists of guided modes or waves, sometimes called Lamb waves [9, 10]. These guided modes can have particle motions (or strains) that are horizontal (SH) or vertical (SV) to the direction of travel. The modes are mainly confined to the steel of the pipe and can travel for long distances. For axial cracks, circumferentially travelling modes are of the most interest because they will broadside the SCC and interact most strongly with them.

Most guided modes are dispersive in that speeds vary with frequency, which causes a pulse of energy to lengthen with time and distance. The dispersion curves in pipe (also plates) depend on the wall thickness, such that the speed variations for a given mode are a function of frequency times thickness [5]. Because of this modes are specified by frequency thickness product (i.e. MHz -mm) and not just by frequency, so that modal properties are relevant to any wall thickness.

Unfortunately, there remain a series of uncertainties concerning the performance of EMAT systems. In particular for EMATs, a deeper understanding of the relationship between material type and the nature of the interacting acoustic and electromagnetic excitations is required, in order to allow the development of advanced systems with better signal to noise ratios, rugged transducers, improved signal processing, enhanced anomaly identification and grading and for more efficient magneto-acoustic coupling. Significant questions concern which type of EMAT and which modes to use and then how to optimise the transducer parameters,

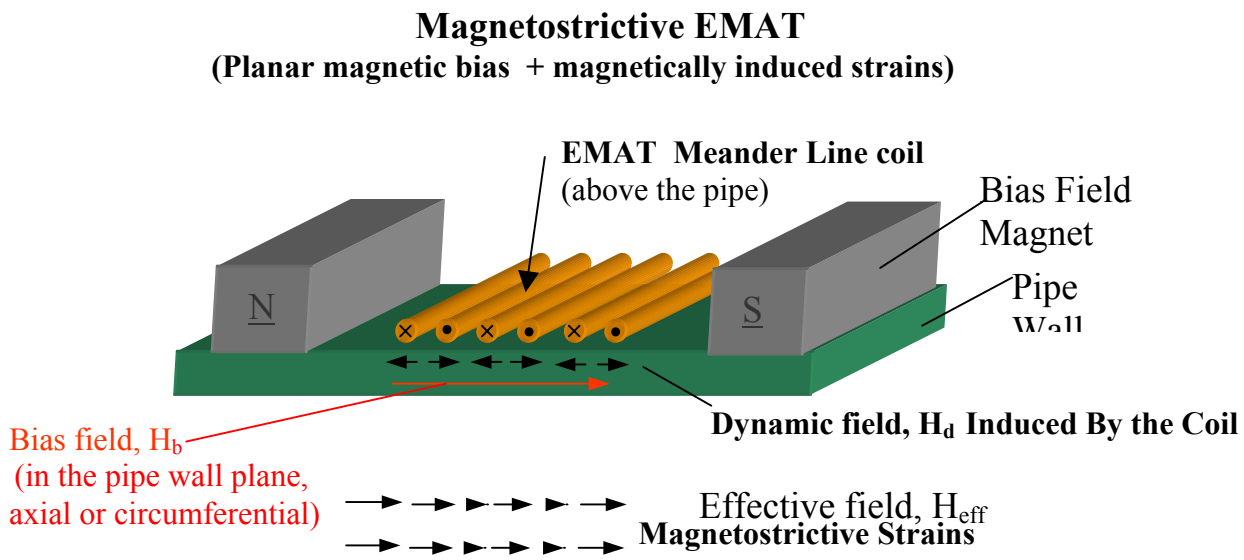

Figure 1 Structure of a Magnetostrictive EMAT Using a Meander Line Coil

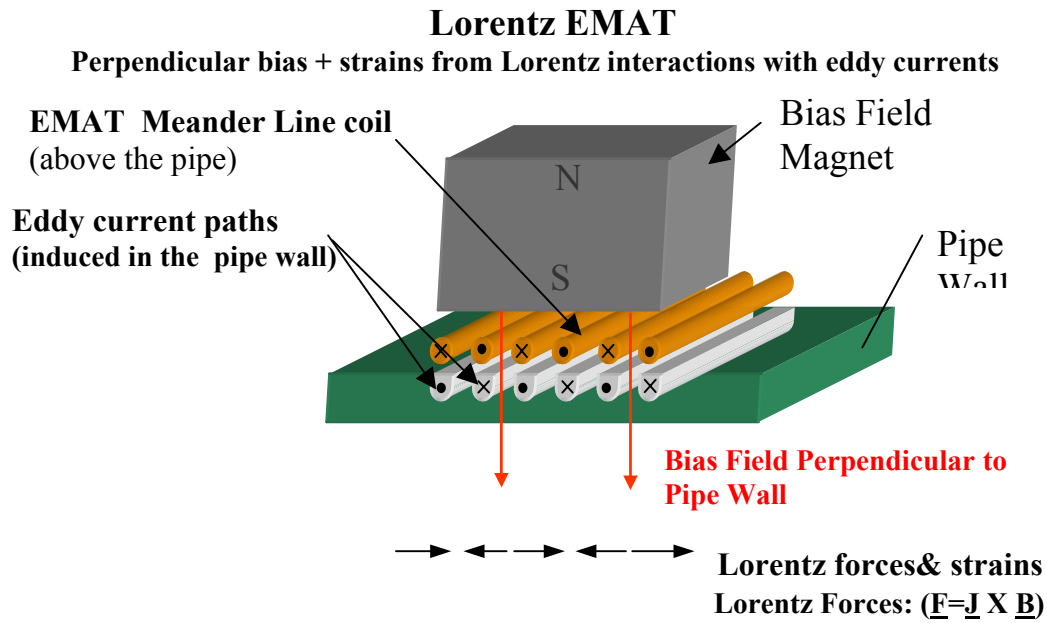

Figure 2 Structure of A Lorentz EMAT Using a Meander Line Coil

such as magnetic biasing, coil length, width, and impedance. Also, there is a lack of understanding about the nature of the acoustic wave interactions with the multiplicity of crack and defect types that can be encountered in gas transmission pipelines.

In this work for DOE, Tuboscope is building on its past work [11, 12] on EMATs in order to develop a suitable commercial system. The method is first to do lab experiments of increasing scale and complexity to find the best modes and frequencies and transducing techniques (magnetostrictive or Lorentz), and next to improve basic transducer responses. Then expand to a more complicated device (lab mouse) that can be manually pulled through a pipe. Expand again to a device (a mule) that is more rugged, closer to commercial, and that can be pulled rapidly in a longer pipe, and finally build and modify a full size commercial prototype.

Previously, a project [12] was completed for the Gas Technology Institute (GTI) in which modelling for guided modes was done for dispersions, for modal shapes, for the reflection and transmission from simple cracks and for the attenuations from the exterior coating and back fill. From this, six modes (at specific frequencies) appeared to be good candidates for further lab study. These had the following desirable properties: low dispersion, high group velocity, high sensitivity to cracks, and low (modelled) attenuation due to the coating. They consisted of two SV modes and three SH modes. They are listed in Table 1.

Table 1 Promising Modes to Pursue For an ILI SCC Tool

Promising SV

Mode	f-d (MHz-mm)	f (MHz)	wl (mm)	Vp (m/s)	Vg (m/s)	Attn 1 (dB/m)	Attn2 (dB/m)	Disp (Y/N) Wavelen (mm)	
SV1	**3.91**	**0.47**	**12.81**	**5956.00**	**4949.00**	**9**	**18**	**12.7**	**N**
SV2	**7.78**	**0.93**	**6.44**	**5959.00**	**4943.00**	**35**	**65**	**6.4**	**N**

Promising SH

Mode	f-d (MHz-mm)	f (MHz)	wl (mm)	Vp (m/s)	Vg (m/s)	Attn 1 (dB/m)	Attn2 (dB/m)	Disp (Y/N) Wavelen (mm)	
SH0	**0.67**	**0.08**	**40.75**	**3260.00**	**3260.00**	**2**	**14**	**40.7**	**N**
SH0	**1.51**	**0.18**	**18.11**	**3260.00**	**3260.00**	**8**	**18**	**20**	**N**
SH0	**2.14**	**0.26**	**12.78**	**3260.00**	**3260.00**	**3**	**8**	**12.5**	**N**
SH1	**2.24**	**0.27**	**17.50**	**4673.00**	**2273.00**	**10**	**23**	**20.9**	**Y**

f-d = frequency-thickness product; f = frequency of excitation in 8.4 mm thick plate; wl = wavelength; Vp = phase velocity; Vg = group velocity; Attn1 = viscoelastic attenuation in plate with a 2 mm coating of coal tar epoxy; Attn 2 = leakage and attenuation in a coated pipe buried in clay (modelled worst-case scenario); Disp (Y/N) = indicated whether or not the mode exhibits dispersion at the excitation frequency.

Their dispersion curves and modelled crack interactions are shown in Figures 3 and 4. Note that the modelling was done by 2 D FEM.

Also as part of the GTI work, a lab system was assembled and an EMAT transmitter for only one mode was built and tested with a piezo receiver. With that system no EMAT receiver was successfully operated and only the SV2 mode had reasonable signal level (with a piezo receiver). However, crack interaction with the single mode was verified, albeit at a low signal to noise ratio. It was clear that significant improvements had to be made in the lab system for the DOE project. This is where this DOE project started, and this report picks up.

This report covers work from the start of the project for DOE in October 2001 until the end of January 2003. It covers the experimental work for vastly improving the lab set up, the picking of the modes to pursue, lab work determining the best biasing and transducer characterization,

lab work with crack interactions on a plate and a curved pipe section, further optimization/adaptation of the EMAT transducers, and initial testing of the lab mouse for a 24 inch pipe.

Additional work now in progress consists of detailed testing of the mouse using real pipe and the design of the lab mule.

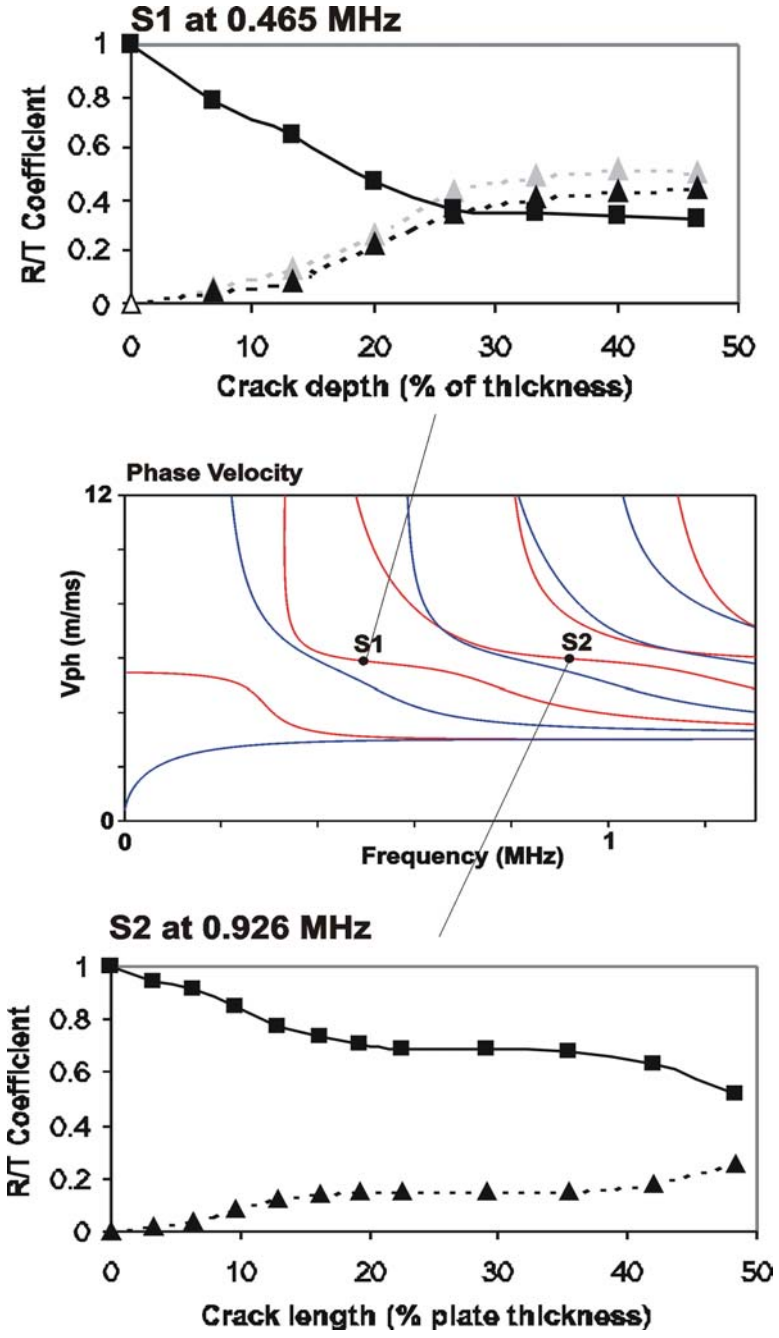

Figure 3 Modelled dispersion curves and crack interactions for SV1 and SV2 modes.

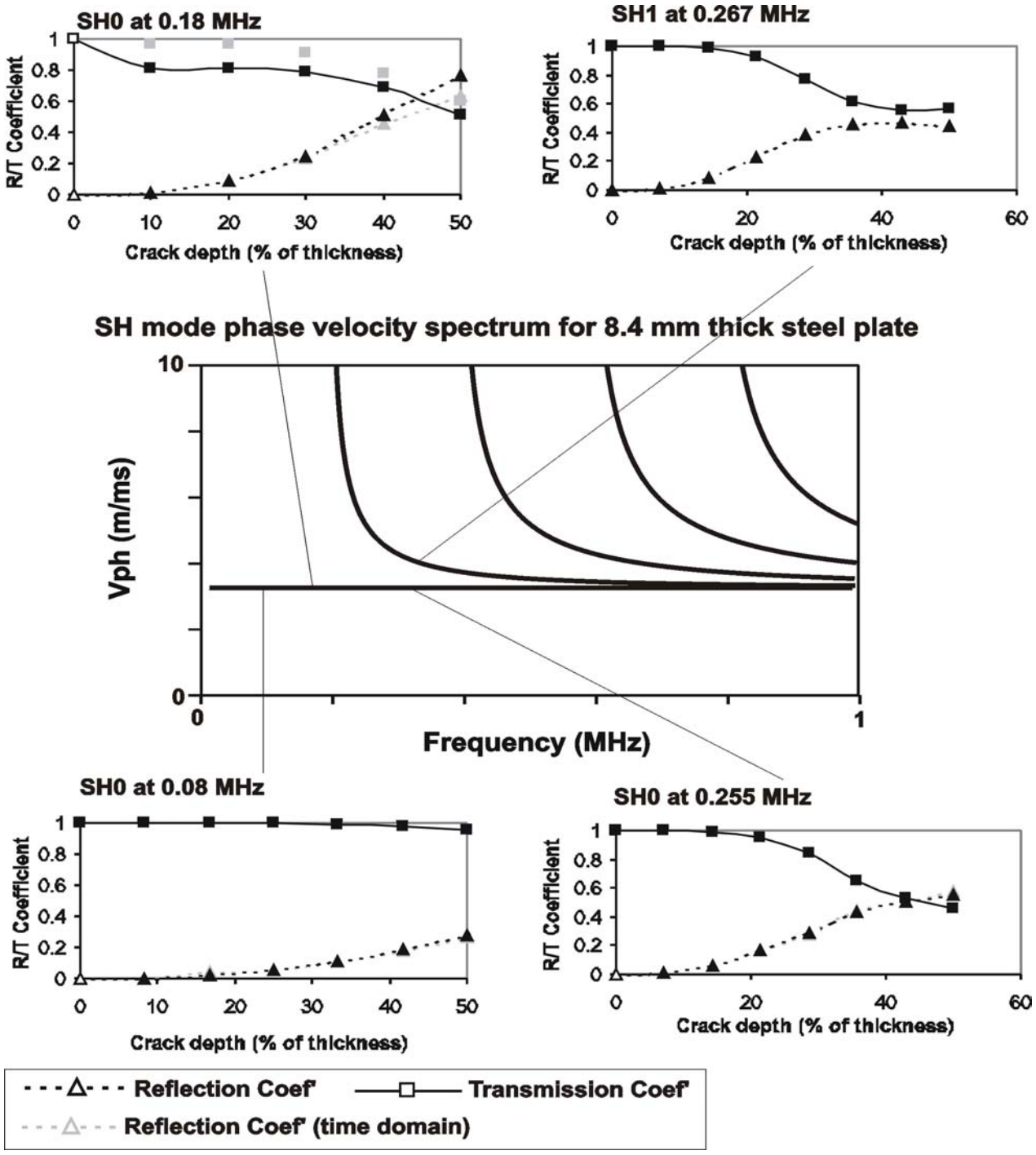

Figure 4 Modelled dispersion curves and crack interactions for SH0 and SH1 modes.

Executive Summary

This report describes progress, experiments, and results for a project to develop a pipeline in-line inspection tool that uses electromagnetic acoustic transducers (EMATs) to detect and grade stress corrosion cracking (SCC). There is a brief introduction that gives background material about EMATs and relevant previous work [12] for the Gas Technology Institute. This work left six choices for the acoustic modes and a choice between magnetostrictive or Lorentz type transducers for this project. A major initial project goal was to narrow these choices via lab work with a flat plate or pipe sections.

The experimental section then describes the lab systems, improvements to these systems, and setups and techniques to narrow the choices. Improvements, which involved transducer matching networks, better magnetic biasing, and lower noise electronics, led to improved signal to noise (SNR) levels. The setups permitted transducer characterizations and interaction measurements in plates with man-made cracks, pipeline sections with SCC, and a full pipe with SCC. The latter were done with a moveable and compact EMAT setup, called a lab mouse, which is detailed.

Next, the results section justifies the mode and transducer choices. These were for magnetostrictive EMATs and the use of EMAT launched modes: SH0 (at 2.1 MHz-mm) and SV1 (at 3.9 MHz-mm). In general, the experience of the improvements and measurement results impacted this choice, which met a major goal. The main justifications were good SNRs and useful crack sensitivity.

The results section then gives details of measurements on these modes. The measurements consisted of signal to noise ratio, insertion loss, magnetic biasing sensitivities crack reflection and transmission coefficients, beam width, standoff and tilt sensitivities. For most of the measurements the section presents useful parametric curves, - for example, reflection coefficient versus crack depth. The section shows scan results for a pipe section having SCC and mouse waveforms from a full pipe in areas with and without a defect. In preparation for a full tool, this section also reviews further coil optimisation and implementation requirements. These involve transmitter and receiver power, acquisition parameters, and magnetic configurations. Further results are beyond the time period of the report.

Finally, conclusions about the improvements, modes, and implementation feasibility are summarized. The significant conclusions are:

- Guided wave modes have been identified and investigated that offer the potential for both detection *and* sizing of stress corrosion cracking sites (SCC). These modes are:
    - The guided wave mode, SV1, chosen at a frequency-thickness (f-t) product (3.9 MHz-mm) such that the mode is (a) non-dispersive and (b) is much faster than other modes at the same (f-t) product.
    - The guided wave mode, SH0 (at 2.1 MHz-mm), which is non-dispersive throughout its range. A frequency thickness of 2.1 MHz-mm has been chosen which allows for reasonable interaction with small cracks. The mode is above the cut-off for SH1, but this is tolerable because the SH1 mode is highly dispersive at this f-t .
- Magnetostrictive type EMATs were chosen because they produced similar SNRs to Lorentz, yet they may be more robust and implementable in an ILI tool.

- EMAT heads[1] have been designed and built for SV1 and SH0 modes to operate in a magnetostrictive manner[2] for the previous f-t products.
- The conclusions below are for magnetostrictively generated SH0 (at 2.1 MHz-mm) and SV1 (at 3.9 MHz-mm), which have the same wavelengths.
- The receiver and transmit heads are identical and operate best under the same high magnetic bias field conditions. That is that magnetic saturation yields the best signal levels.
- SNRs of >100:1 and ~30:1 has been achieved for SV1 and SH0, respectively with a stand-off of ~.1mm, high bias field (magnetic saturation) conditions, and a peak drive current of ~10 A for the transmit EMAT coil using a double-layer coil in series.
- The amplitude decrease upon standoff (and tilt) of the EMAT coils has been determined. A standoff of 2 mm could be tolerated or mitigated by the use of a higher drive current.
- For the EMAT coil geometry[1] described here, beam characteristics have been measured. There is very little beam divergence up to ~500 mm distance from the transmit EMAT head; the beam width is approximately that of the transducer; there are no side lobes.
- The interaction of these modes with narrow, but axially long cracks on a flat plate has been measured and compared to modelled results. The experimental results agree reasonably well with the predicted results.
- The reflection and transmission coefficients (both measured and modelled) of SV1 and SH0 show promise for grading crack depth. SV1 is sensitive to shallow cracks, while SH0 is sensitive to deeper (>20% wall thickness) cracks.
- Crack interactions on pipe sections, although they indicate some interactions for transmission, are inconclusive for reflections and indicated a need for full pipe experiments.
- An EMAT mouse system capable of scanning 24” OD pipes (wall thickness of 8.4 mm) using both SV1 and SH0 heads has been designed and built. Initial waveforms have good SNRs and good modal purity.
- For the EMAT mouse, easily discernible reflections with appropriate arrival times indicate promising crack interactions. These justify pushing ahead with complete scans for SH0 and SV1 with the mouse. These will be described in the next major report.
- Acquisition, power, and magnetic configuration requirements for a full-scale mule or ILI tool have been considered and are reasonable.

[1] ~80 mm wide (axial direction w.r.t. to pipe) by ~60 mm long (circumferential pipe direction).
[2] In-plane circumferential bias for SV1. In-plane axial magnetic bias for SH0.

Experimental

Flat Plate Lab Set up and Improvements

Work was initially done to improve the lab system from the GTI project. The system had to be capable of digitizing waveforms with good SNRs. It needed to have flexibility to handle various geometries and frequencies and biasing. This was then used for the following measurements or investigations on a flat plate of pipeline steel: transmitter output and sensitivity variation with magnetic biasing, receiver sensitivity, signal to noise ratio, pitch/catch insertion loss, crack interactions (reflection and transmission coefficients).

The final, improved, lab system, is shown in Figure 5 and diagrammed in Figure 6. Improvements over the GTI system consisted of the following: EMAT receivers, efficient impedance matching networks for transmitters and receivers, new magnetic bias magnets and a bias supply that yielded increased magnetic biasing fields (more amp-turns) and more uniformity of magnetic bias, a new preamplifier that reduced noise and breakthrough, new EMAT coils with reduced losses, and complete grounding and shielding that further reduced noise.

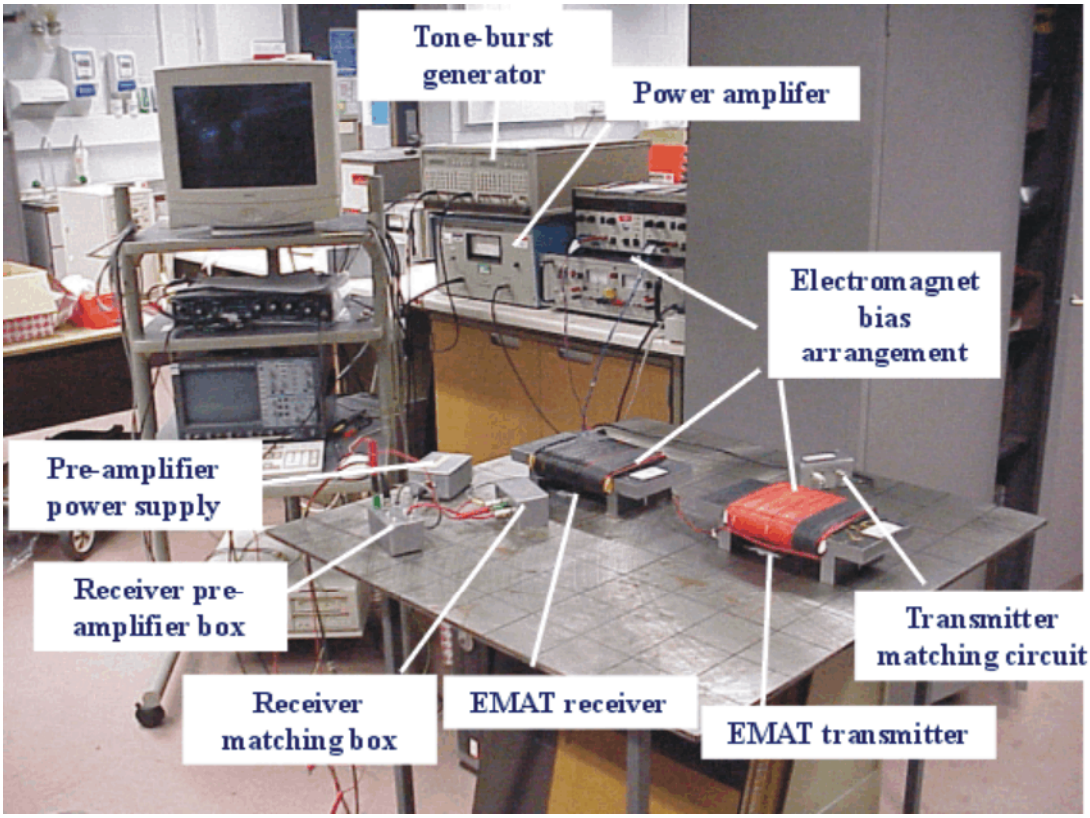

Figure 5 Laboratory set-up of the pitch-catch experiments using SV1 EMAT heads biased for magnetostrictive coupling.

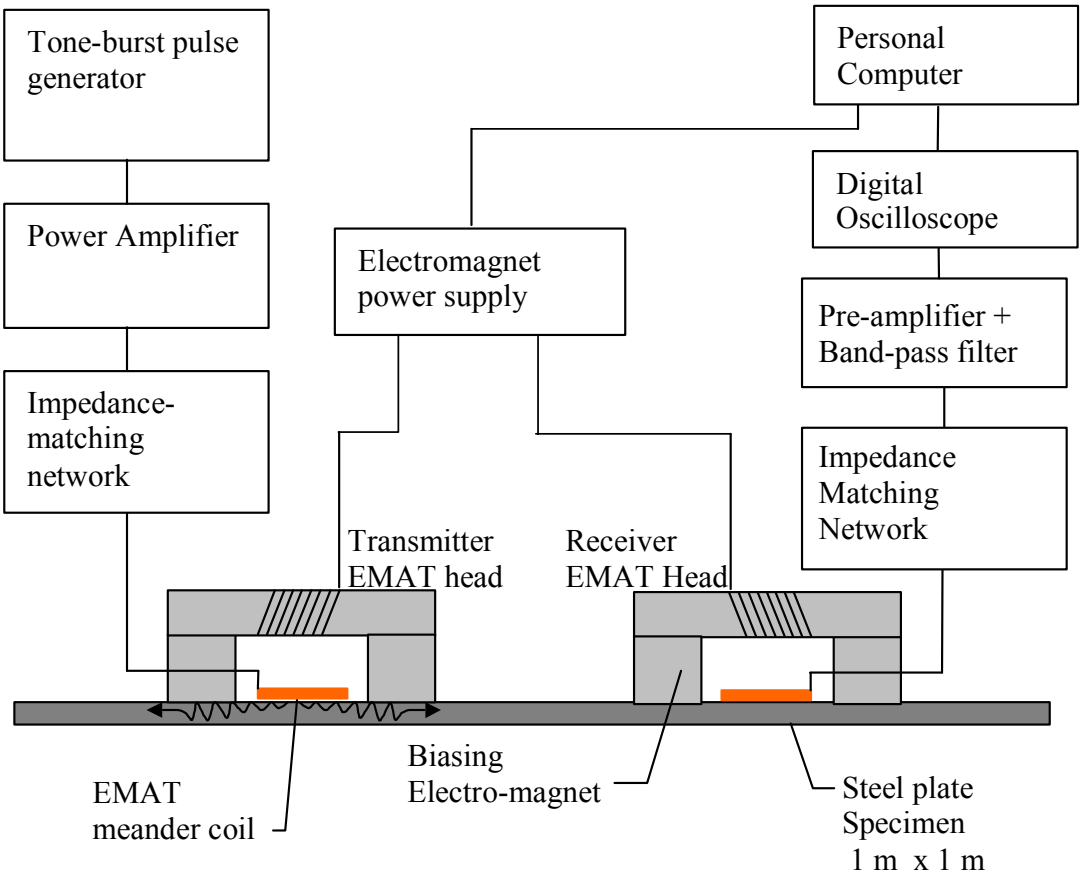

Figure 6 Schematic of the lab set-up used in most experiments (in pitch-catch configuration)

This system, had separate EMAT heads and biasing for both the transmit and receive heads and operated in pitch-catch mode. This approach not only simplified the electronic circuit design but was also necessary if the optimum biasing was different for transmitters and receivers.

For all flat plate measurements the plate was one meter square and 8.4 mm thick of pipeline steel. It was supported at the edges by wooden legs.

The new biasing electromagnets carried about 800 turns. They were capable of 10,000 Amp-turns and their pole pieces rested on the plate. Later they could be modified to provide axial or circumferential biasing in the plane of a pipe. The DC supply, which was computer controlled, allowed the plate and the poles to be degaussed before any measurements were taken. Degaussing was done for all flat plate measurements.

It became apparent during early tests that magnetostrictive EMATs required an axial magnetic bias for SH0 and a circumferential for SV waves. This is diagrammed in Figure 7.

The EMAT coils were flat, single layer meander line (ML) patterns of 5 periods (10 "fingers'). They fit between the poles of the bias magnets. A final version is shown in Figure 8. For the

Static Magnetic Biasing For Magnetostrictive EMATs

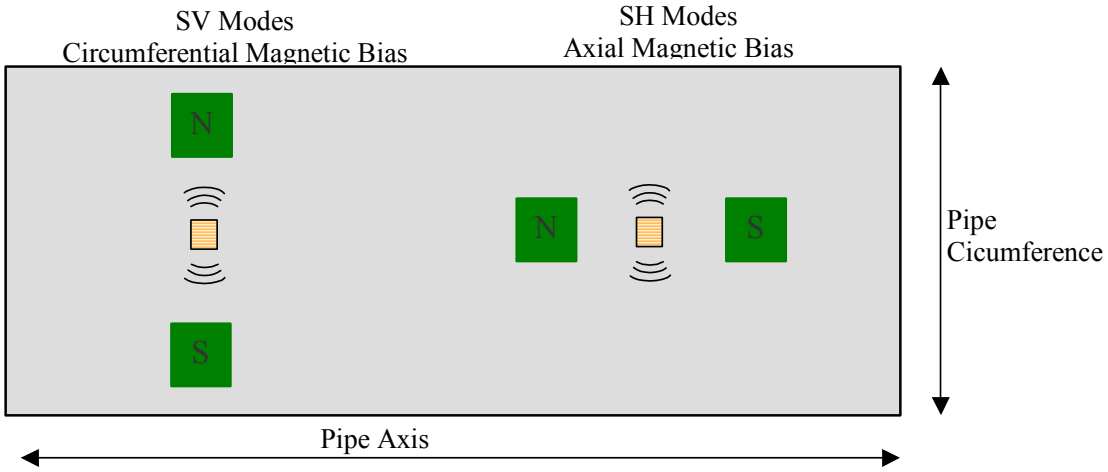

Figure 7 Magnetic bias field geometry relative to wave propagation For magnetostrictive EMATs

final work, concentrating on the SV1 and SH0 modes, the coils were 80 mm wide by 60 mm long. Coil traces and contacts were optimised and thickened for minimal resistance for a given period, number of wavelength (loops) and coil width. Coils were first manufactured using etched PCB circuits. Flexible heads, which are necessary for curved specimens such as pipe sections, were later produced by etching polyimide-backed copper of 70 μm.

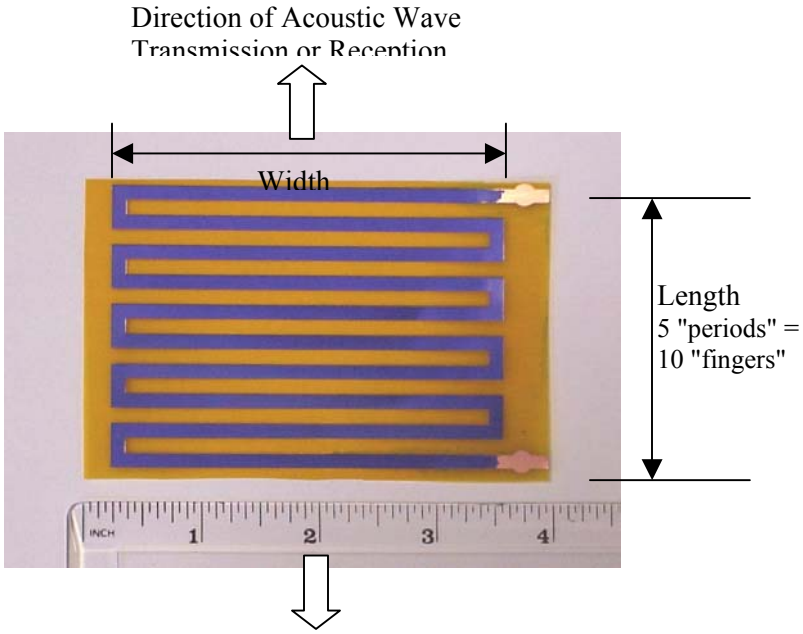

Figure 8 Example of the meander line (ML) EMAT coil used in this work.

Some investigations were also done with periodic permanent magnet (ppm) EMAT heads and pancake coils.

A general purpose lab RF power amp could supply more than 35 A (after matching) of frequencies from 100 kHz to 1 MHz. Because the power amp had a fixed 50 ohm output impedance, while the EMAT was 1 ohm or less, a matching network was required to efficiently couple the amp to the EMAT. Without good matching, the amp would not supply sufficient current to the EMAT, and signal amplitude, which is proportional to transmitter current, would be degraded. For maximum power transfer the EMAT was coupled to the power amp through an LC matching network. This was resonant, so a different network was made for each frequency investigated. For best signal characteristics the matching networks were in compact shielded boxes with shielded leads to the EMAT and preamp as short as possible.

For all measurements the EMAT was driven by a five cycle tone burst at the center frequency of the mode being investigated.

Note that there is also matching requirement for the receiver to the input preamplifier. In this case the matching network steps up the impedance and voltage of the source, so as to match an optimum impedance for the noise generated in the circuits of the preamplifier. The preamp required a match to 100 ohms, which was done by a different resonant LC network for each frequency.

The special low noise, high gain preamp was key in improvement of signal to noise ratios. The preamp, which was developed, provided 90 db gain followed by high and low pass (6 pole) active filters. The latest design had a switched center frequency (either 260kHz or 470kHz) and band width. This was packaged in a shielded box with extra supply filtering.

Measurements and Investigations

Crack Interaction and Modal Content

In all cases the captured signal has been analysed to verify that it represents the desired wave mode. This has been undertaken first by analysing the time of flight of the received wave packet and comparing it to the expected time of flight based on the group velocity of the guided wave of interest. In all cases a good match was found. Second, the dispersion characteristics of the received wave packets were examined in detail. The guided wave modes that were being investigated are non-dispersive at the specified frequency-thickness product. By altering the frequency of the input signal up or down from the specified frequency it was possible to observe the received wave packet becoming dispersive. This confirmed that the received wave packet is indeed non-dispersive at the expected frequency, further confirming it is the desired wave mode

For initial crack interactions, reflection and transmission coefficients were measured from a man-made crack in a flat plate. Figure 9 shows the geometry. Note that to avoid EMAT head beam width effects, the crack was very long (500 mm) compared to the width of the EMAT head (typically 80 mm). This was the situation for the modelled results in figures 3 and 4, so that theory could be compared to measurements.

All amplitude measurements were based on peak to peak measurements of digitized received signals. For example, for reflection coefficients, the direct arrival and reflection wavelets were identified in a received waveform by means their arrival times, based on the mode group velocity and distance to crack. Then their peak to peak amplitudes were measured. The reflection coefficient was taken as the ratio of reflected peak to peak divided by the direct arrival peak to peak. For a transmission coefficient, the direct arrival peak to peak for a given crack was divided by the peak to peak for no crack. Thus, no crack would have a transmission of 1.

.

Note that dispersion, biasing, signal to noise, insertion loss, beam width, standoff and tilt sensitivity measurements were all made with transmission configuration (Figure 9 A without a crack) but at a different separation between transmitter and receiver heads.

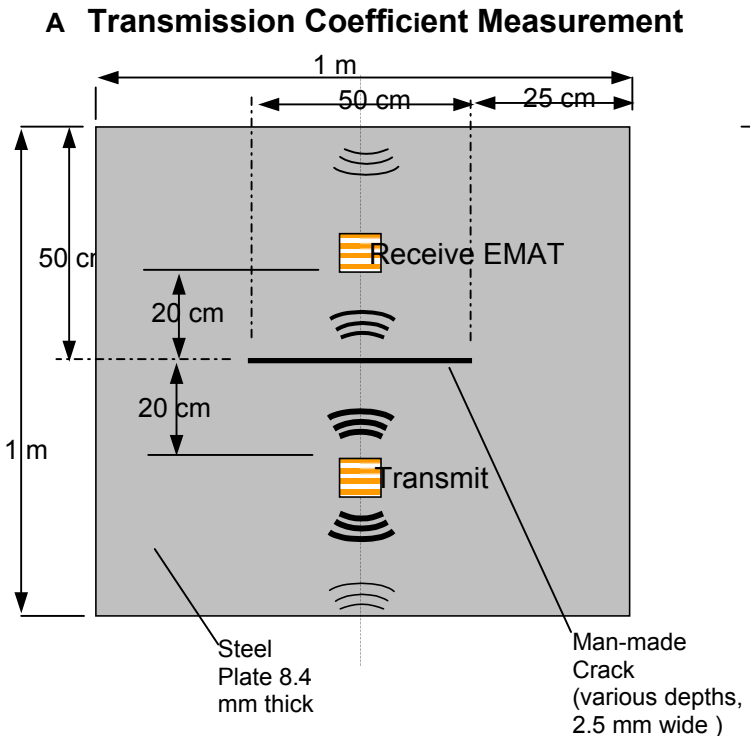

Figure 9 A Flat Plate Crack Transmission Interaction And General Pitch Catch Geometry

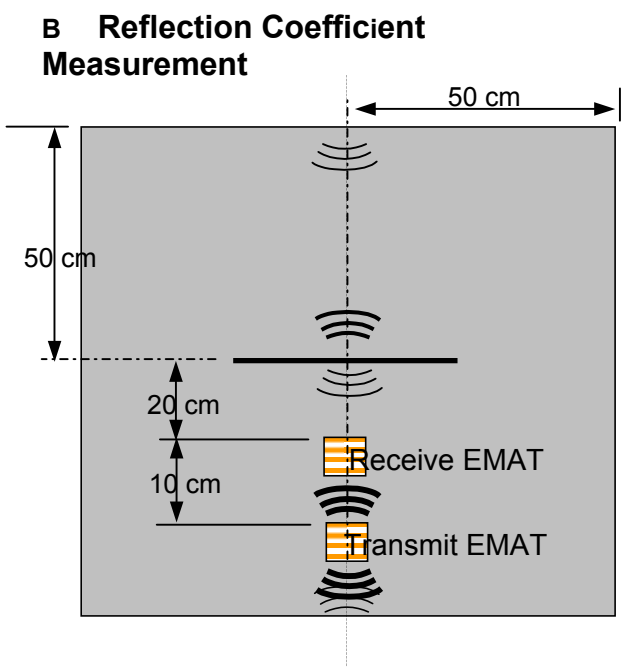

Figure 9 B Reflection Crack Interaction Geometry

Beam width at operation frequency

Two experiments were undertaken to characterise the beam width of this transducer. In the first instance the EMAT receiver coil was moved relative to the EMAT transmitter coil, as shown in Figure 10, at increasing propagation distances.

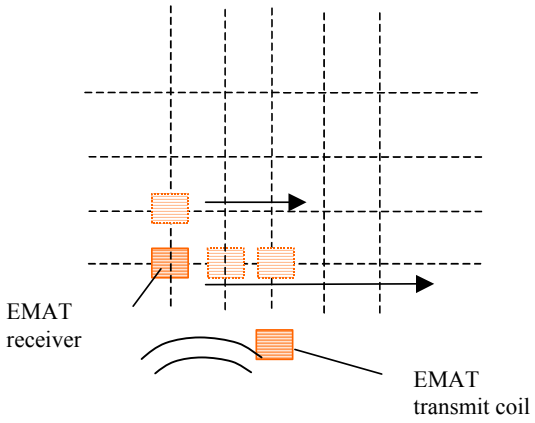

Figure 10 Measurement of beam width of SV1 mode by receiver translation.

In the second experiment the transmitter and receiver coils were kept in line while measurements were taken (at two different propagation distances) as the transmit coil was rotated (Figure 11).

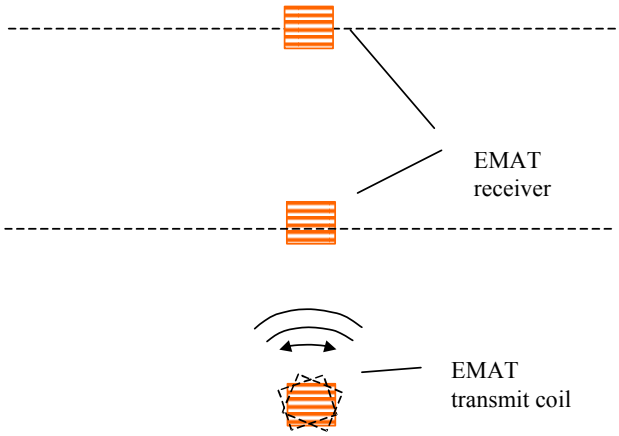

Figure 11 Measurement of angular dependency of SV1 mode by transmitter rotation

Sensitivity To Standoff and Tilt

These were done on the flat plate set up using the SV1 EMAT coil only. For these investigations the receiver and transmit coil were independently raised from the surface of the steel plate. While one transducer was lifted vertically from the plate, or tilted, the other transducer remained about .1 mm from the plate surface. For tilt, one edge of the moved transducer rested .1 mm from the plate while other edge was lifted. Both side to side and front to back tilting were done. We could work with SV1 only because we verified that the amplitude versus standoff depended on wavelength. Because the SH0 and SV1 waves at the frequencies to be investigated had nearly the same wavelengths and because the coils were same, results for the SH0 EMAT coil will be identical.

Experiments were undertaken on a flat plate to investigate the effect of the bias field for both the transmit and receive EMAT coils on the received signal amplitude of the desired wave mode. The transmitter and receivers were set in line 20 cm apart on the defect-free flat steel plate. Note that the received signal amplitude (peak to peak) was recorded as bias current for one transducer was varied (in steps), while the other was held at a fixed value. This was done for a fixed, but high EMAT RF drive voltage. Thus, signal amplitude response to transmit and receiver bias were determined separately.

SCC Crack interaction Measurements

Experiments were carried out on the SCC samples cut from pipe sections. Modification of the bias field set-up and the manufacture of flexible EMAT coils was necessary in order to carry out this task. An example of the experimental set-up is shown in Figure 12. The pipe section was cut from a 30" pipe of .312 wall dug for an actual pipeline due to the occurrence of SCC. The section was 1 meter axially by about .80 meters of arc. The SCC defects are denoted by circled areas and marked F90, F93, and F106. These were families of small cracks.

The set-up geometries for this series for transmission and reflection experiments are shown in Figure 13 and 14, respectively. For both SV1 and SH0, circumferential waves were launched. The difference for between SH0 and SV1 was the magnetic biasing: axial for SH0 and circumferential for SV1. For SV1 different poles pieces were fitted to the electromagnets, which were turned by 90 degrees. The flat plate drive and acquisition system was used for these measurements.

Figure 12 Experimental set-up for SCC interaction with SH0 mode using pipe segments.

Waveforms were taken at 11 axial positions, with the transmitter and receiver aligned. The positions are spaced by 2.5 cm. Time in each waveform corresponds to circumferential distance. In most cases the waveform was an average of 100 shots at the same position.

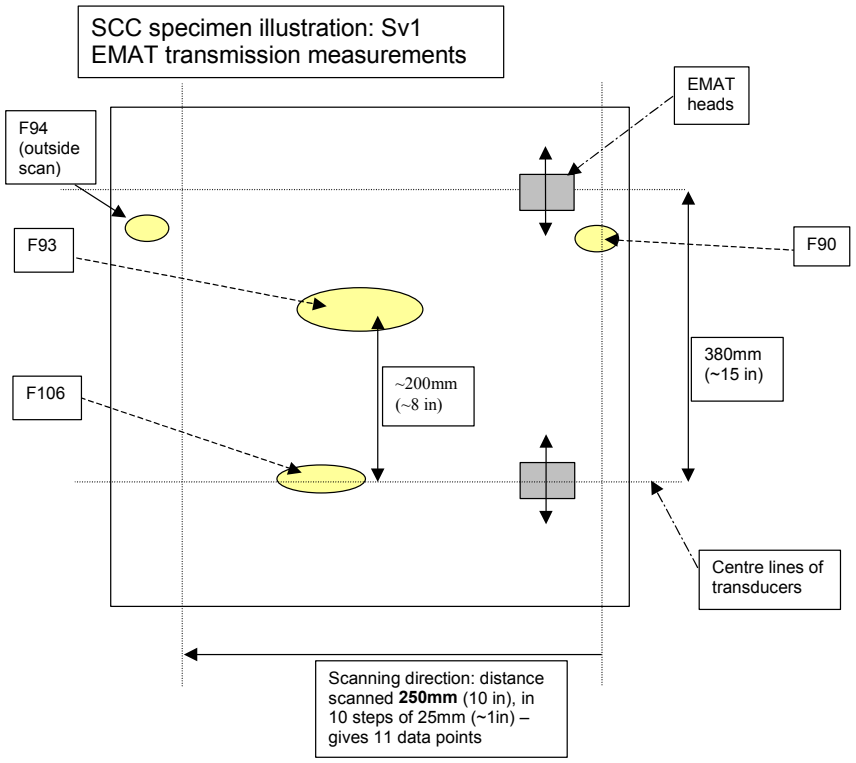

Figure 13 Set-up for determining interaction of SV1 guided wave mode with SCC sites in transmission.

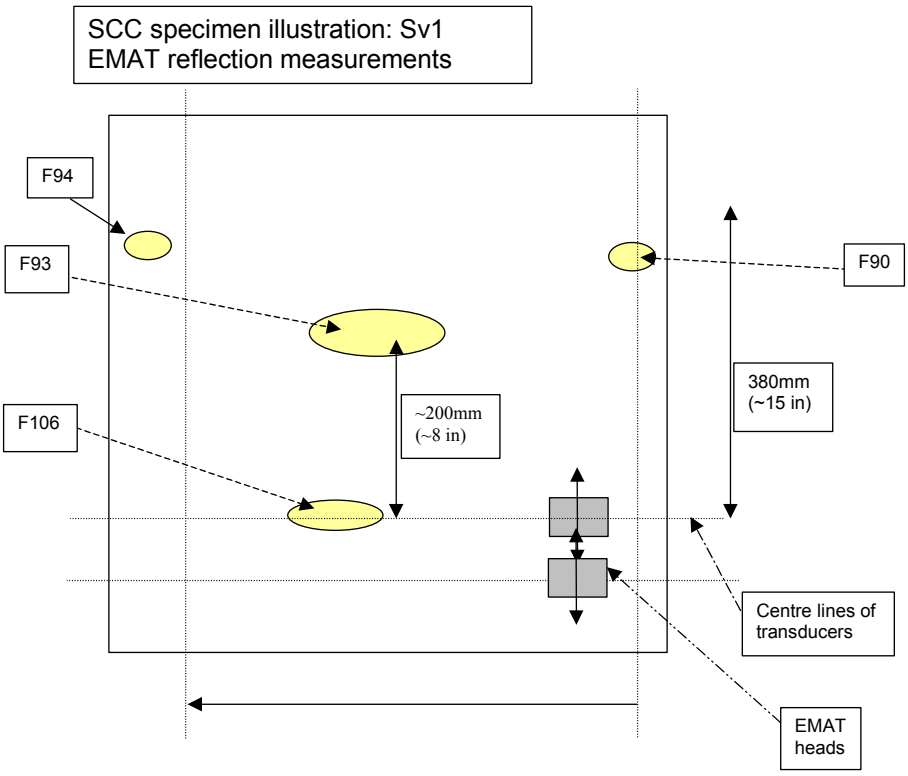

Figure 14 Set-up for determining reflection interaction of a guided wave mode with SCC sites

Lab Mouse

One of the key conclusions of previous work was that the mouse should investigate both the SV1 and SH0 modes. Consequently the mouse needed to be able to accommodate the different magnetic bias configurations, as per Figure 7. The mouse utilised the existing electromagnets (with small modifications to allow them to fit into the pipe curvature) from the previous flat plate experiments.

The test mouse design was based on a carrier to hold the electromagnets and coils of both the transmit and receive EMAT heads in close proximity to the inside pipe wall which could be moved along the pipe sample on rails. Two carriers were made to either hold the electromagnets for axial magnetic field bias (SH0) or for circumferential field bias (SV1). The material of construction for the carriers and rails was chosen to be wood since it is (a) non-magnetic, (b) non-conductive, (c) highly damped, (d) versatile and (e) cost-effective. Thus, it would not support or propagate stray or confusing ultrasonic signals. The carriers would be manually moved down the pipe axis to a sequence of stations to simulate the scan of a completed measurement system. Station measurements would be taken with the carrier, in a step, measure, and repeat fashion.

Various photos of the EMAT mouse system are shown in Figures 15 through 19.

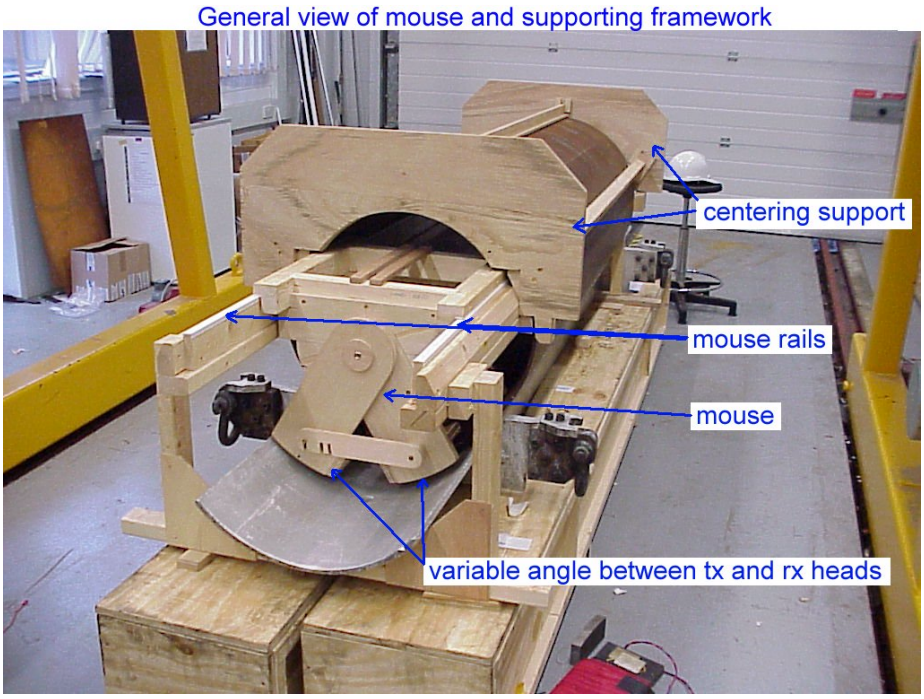

Figure 15 Overall view of the EMAT mouse set-up showing the SH0 carriage being loaded into the pipe.

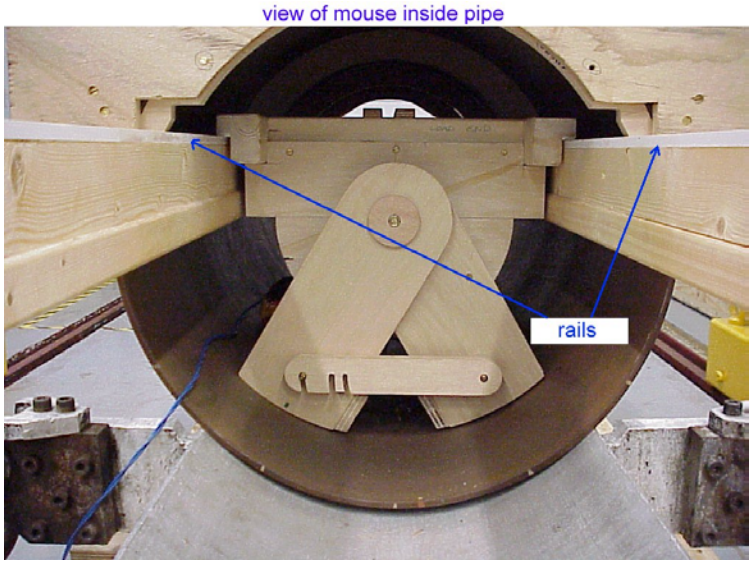

Figure 16 Cross-section view of the SH0 carriage in position in the pipe.

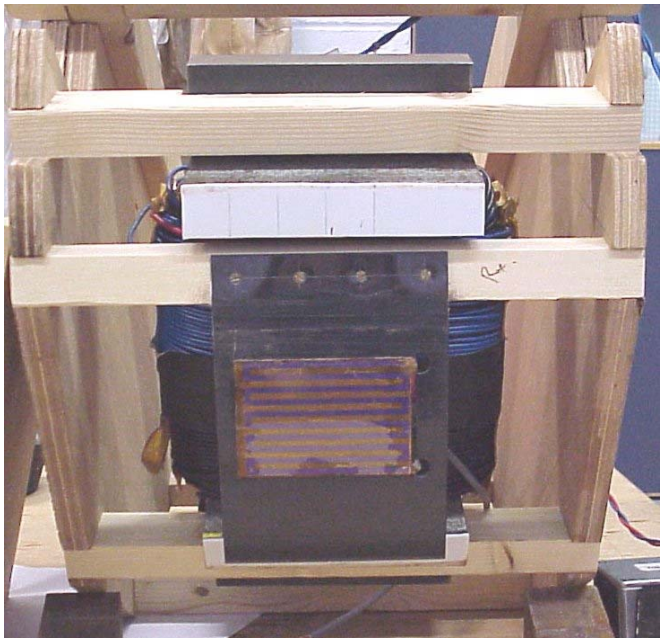

Figure 17 Side view of the SV1 carriage showing the meander line (ML) coil and electromagnet in position.

EMAT heads were produced based upon the coil design described in earlier sections. For the EMAT transmitter head two layers of polyimide backed copper meander coils in series were used. The coils were mounted on a polymeric substrate that had been vacuum formed to the curvature of the pipe specimen being examined (pipe sample P2 - 24" OD). A thin polymeric coating (acetate) was applied to the underside of the coating to provide both electrical isolation and some degree of protection for the EMAT coil. A view of the EMAT heads mounted on to the mouse is given in Figure 17.

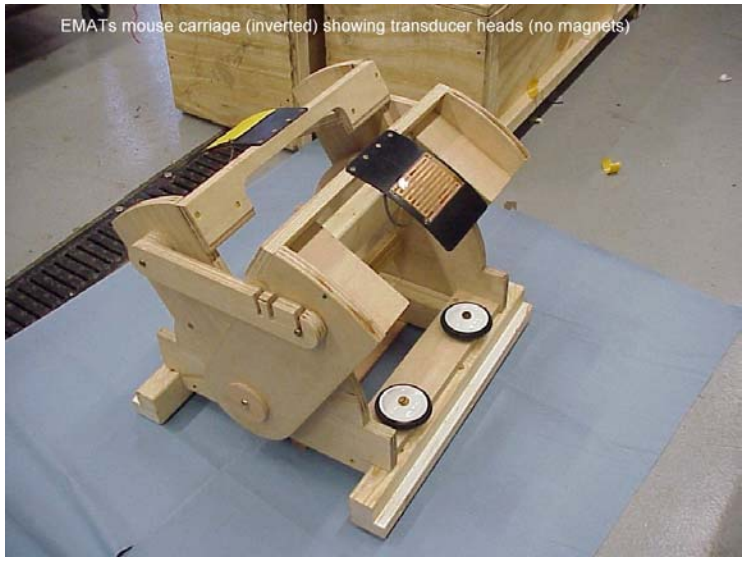

Figure 18 View of the EMAT heads mounted on the SH0 mouse carriage (inverted).

The data acquisition system was an enhanced version of the flat plate system. Its block diagram is identical to that of the plate test system in Figure 6. The matching networks were mounted on the moving mouse. The rest was remote, so cables were run to the electromagnets and the EMAT heads. Figure 19 shows a view of that system.

Figure 19 Overall view of the EMAT System including ancillary equipment for signal generation, data capture and data analysis.

Three software programs were written, in Labview, in order to capture and analyse the data from the mouse experiments. The programs were:

(1) 'EMAT 1b' – this software package communicates with the electromagnet power supply allowing the user to vary either (or both) the transmit or receive bias fields. The program also

communicates with the digital oscilloscope and will capture the time traces collected by the oscilloscope and store them into defined (.tim) files.

(2) 'EMAT 1b Animation Analyser' – this package allows the user to import all of the data (.tim files) captured during an experimental sequence (e.g. the scan of a pipe or bias field variations). The program can then animate the changes in the timetrace during this sequence of experiments and carry out simple analysis of the data (e.g. maximum peak amplitude over a defined time window) throughout the sequence. This was the main program for scanning the pipe. A screen capture is shown in figure 20.

(3) 'EMAT 2' – this is a designated software program that carries out a bias field sweep using the electromagnets of either the transmit or receive EMAT head (or both) while capturing timetraces at specified field (current) intervals.

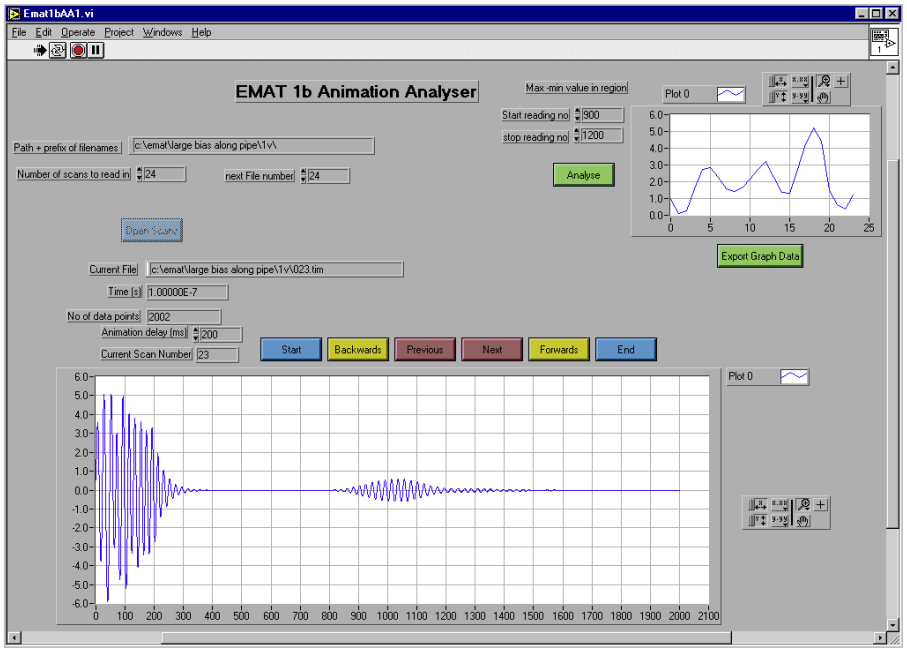

Figure 20 Screen capture of software program 'EMAT 1b Animation Analyser' used for logging the pipe.

A 24 inch diameter pipe sample, designated P2, was chosen for the pull-through tests as (a) it was uncoated, (b) had eight defects along a line that could be clearly visually identified, but (c) otherwise appeared to be defect-free. The positions of the defects are shown in Figure 39.

The set-up for the reflection series of experiments is shown schematically in Figure 21. The defect line is counter-clockwise from the receiver. In this arrangement, the receiver EMAT head (Rx) will first receive the direct signal (travelling counter-clockwise) from the transmitter (Tx) followed next by any reflected signals from the line of defects P2-1 to P2-8. The next signal received will be the back-propagated wave from the transmitter (travelling 270 degrees around the pipe circumference clockwise).

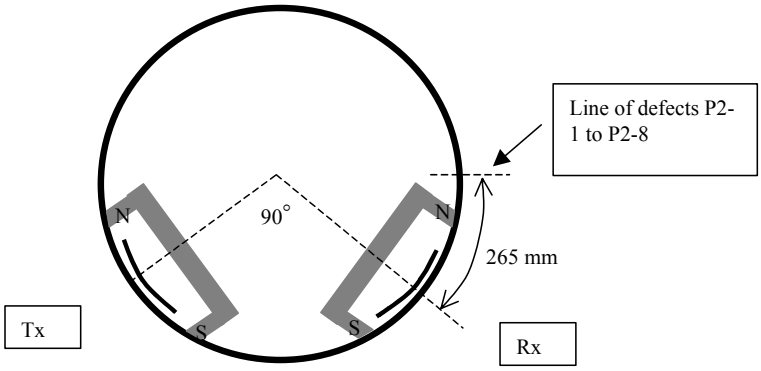

Figure 21 Schematic of the 'reflection' experimental set-up used to scan pipe sample

The set-up for transmission experiments is shown schematically in Figure 22. The defect is clockwise from the receiver. In this arrangement the receiver EMAT head (Rx) will receive the direct signal from the transmitter (Tx) after it has interacted with the line of defects and travelled counter-clockwise 90 degrees.. The next signal received will be the back-propagated wave from the transmitter (travelling clockwise 270 degrees around the pipe circumference) which will not have traversed any defects. This back-propagated wave may therefore be used to normalize the direct arrival in order to compensate any transmission loss and coupling effects in the direct signal.

Note that the angle between the transmitter and receiver EMATs could be varied from 45 to 90 degrees. The smaller angle is better for reflection measurements, while the wider is better for transmission measurements.

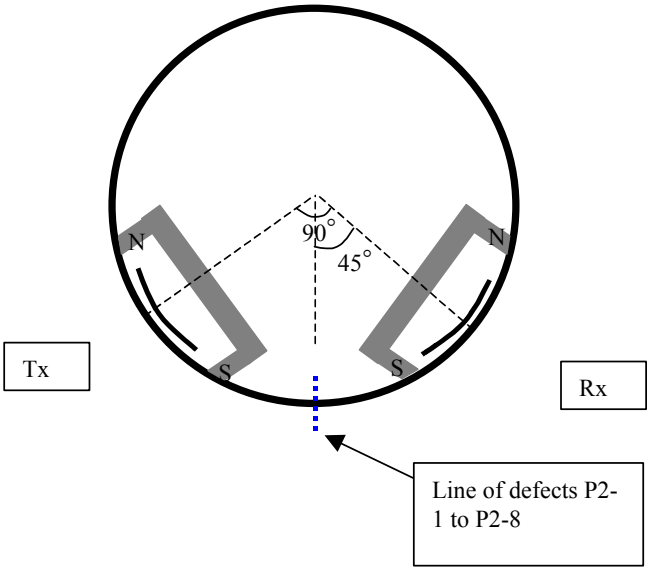

Figure 22 Schematic of the 'transmission' experimental set-up used to scan pipe sample P2

Results and Discussion

Best Modes and Transduction Type To Pursue

During and just after the lab improvements phase we tried both Lorentz and magnetostrictive transduction. The choice criteria for transduction are for good signal to noise ratio, robustness and the practicality for implementation.

Although signal to noise ratios and power were similar for both, we decided to pursue magnetostrictive, because it had additional advantages. First, magnetostrictive allows the bias magnets to be separated from the EMAT coil. Thus, a light ML coil could be sprung without a heavy load on it, and the bias magnets, surrounding the coil , could even provide some protection. This is a much more rugged situation than occurring for a Lorentz EMAT, which must have the bias magnet above the coil. Another advantage of the magnetostrictive is that the bias field required is in the plane of the pipe, and so it is easier to establish than the than perpendicular field required by a Lorentz EMAT. The Lorentz magnet arrangement (Figure 2) will be also larger than the magnetostrictive radially, making it more expensive and less able to accommodate diameter restrictions. Finally in flat plate tests, we observed more complicated waveforms and more dispersion for Lorentz transducers, which indicated less modal purity for Lorentz. This was probably due to the fact that its bias field was diverging from perpendicular.

Because it would be impractical to implement all six of the candidate modes in Table 1, we had planned to narrow the list to one or two of them. The criteria for modes were low dispersion, a high sensitivity to cracks, ease of implementation, limited size of the EMAT head, low sensitivity to standoff and tilt, low expected attenuation, good modal purity and minimal interference from other modes.

Based on these criteria, we decided to pursue further the SV1 mode at 470 kHz and the SH0 mode at 260 KHz. Two modes were chosen in case one choice led to a blind alley and because they had complimentary crack sensitivities. The latter behavior is that SV1 was sensitive to shallow cracks, while SH0 is sensitive to deep cracks. Both had good to excellent SNRs. The SH0 had a disadvantage of a lower signal to noise ratio, but the theoretic advantages of less attenuation and of simpler crack interactions[3]. Compared to SH0, the SV1 mode had a higher SNR and group velocity and required less power, although it was very slightly dispersive and prone to attenuation from the exterior coating. We could not eliminate either mode because in all other factors they weighted similarly. For example, both could be easily excited and had nearly the same wavelength. Thus, we decided to pursue both at least through the mouse tests.

The other modes were easily eliminated due to one or more major failings. The SH1 mode could not be generated and SH0 mode (at 67 kHz) could not be generated with decent SNRs. The SV2 mode was too high a frequency to easily generate and could have much higher attenuation due to coating. Its wavelength was very short. Thus, it would be prone to standoff and beam spreading. The SH0 modes at .67 and 1.15 MHz-mm would have wavelengths too long, making their meander coils impractically large. Thus, they would be prone to damage and poor axial resolution.

[3] This because SH modes should not convert to other modes at boundaries between materials.

Lab Improvements and Transducer Measurements

To save space in this section we concentrate on the previously mentioned chosen transduction type and modes. These are magnetostrictive and SH0 at 260 kHz and SV1 at 470 kHz. Note that measurements of some properties were irrelevant due to low SNRs or the dependence of those properties on wavelength or generic mode type (SH or SV).

Matching Network

The matching network steps down the amp impedance and as a consequence steps up the current supplied to the EMAT. It therefore follows that the lower the impedance of the device and the larger the initial impedance mismatch, the larger the available current step up when the impedance is matched. This was confirmed experimentally, as shown in Figure 23, in which the current flowing through the transmit coil was measured for several different EMAT coils, each with a different impedance value. The agreement between measurements and the curve indicates low losses in the matching network (i.e. high efficiency).

Although this would indicate that the lower the EMAT resistance, the better, it should be noted that if the resistance value gets too low, the Q of the matching circuit becomes very high. At this point, we found that high circuit stability and ruggedness is hard to achieve. Additionally, the acoustic signal will be proportional to the number of turns in the EMAT coil. Consequently for optimum signal output there will be a trade off between the number of turns and the resistance of the coil for optimum coupling (and hence drive current). For the coils used for SH0 and SV1 this was about 1 to 2 ohms.

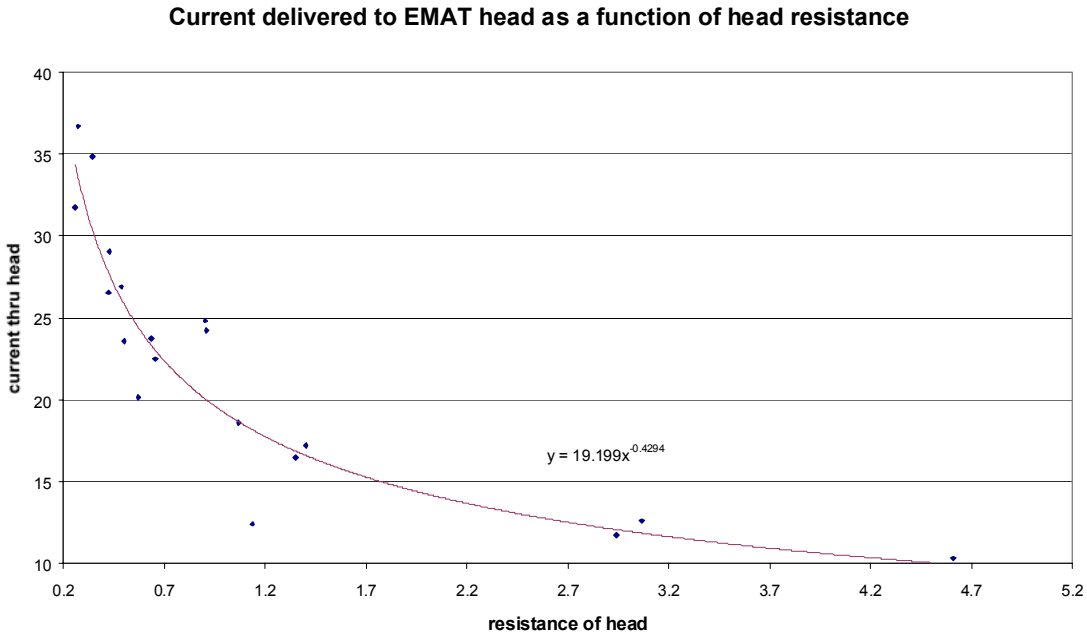

Figure 23 Measured current flowing through the various transmit EMAT coils using a 100W maximum 50Ω source.

Signal to Noise and Insertion Loss

With the improved flat plate set-up the sensitivity of the receive EMAT coils was significantly increased. This was especially so for the SV1 3.91 MHz-mm mode in which a "live" (unaveraged) signal to noise ratio (SNR) of ~100:1 has been achieved using a single-layer transmit coil. An example trace of a directly received SV1 toneburst is given in Figure 24. In this case the drive current for the transmit coil was measured at 25 Amps (peak). The insertion loss for this arrangement was calculated to be ~ 120 dB.

SNR for the SH0 EMAT receive heads was initially less than 1, with the result that SH0 could hardly be observed. After improvements, the live SNR ratio of ~30 to 1 was achieved. In this case the drive current for the transmit coil was measured to be 22 Amps (peak). An example trace of a received toneburst of the SH0 mode at 2.14 MHz-mm is shown in Figure 25. The insertion loss was about 130 db.

All of the work described above was carried out using meander line (ML) EMAT coils of the type and size shown in Figure 7. It was thought that for the SH modes, increased sensitivity and improved insertion losses may be achieved through using pancake EMAT coils with periodic permanent magnets (ppm heads). One drawback of this type of head is that the bias magnets and their extra mass are directly behind the coil. Some preliminary work has been carried out on ppm-SH heads. Although the SH0 mode can be transmitted and detected using these heads, no significant improvement to insertion losses was apparent. Thus, considering the drawback of their extra mass, further development was dropped.

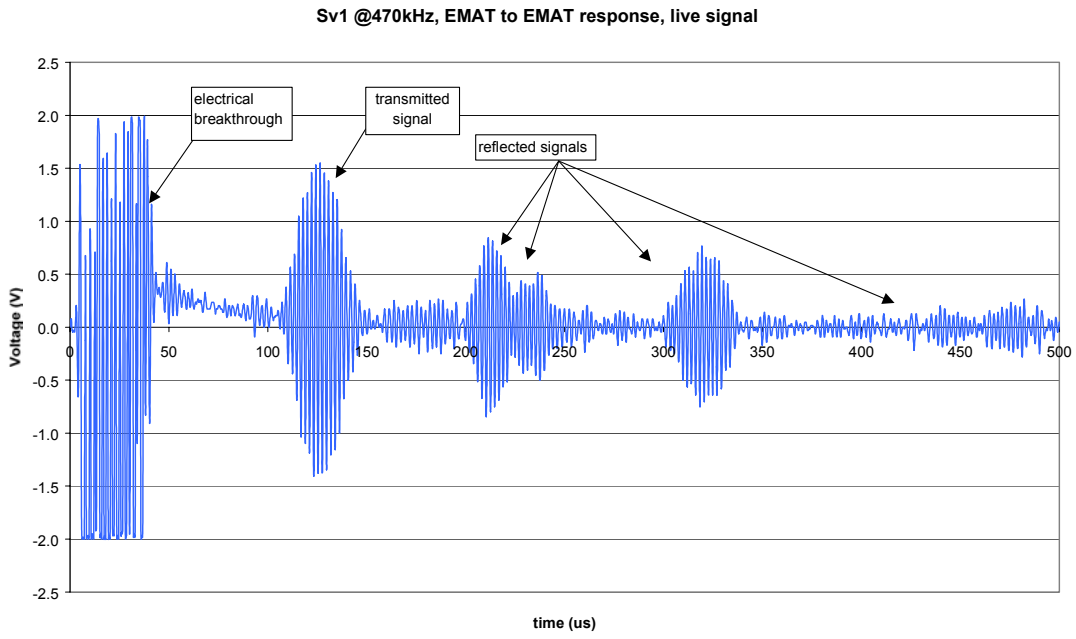

Figure 24 Example trace of the live received signal from a SV1 toneburst; reflections from the plate edges are indicated

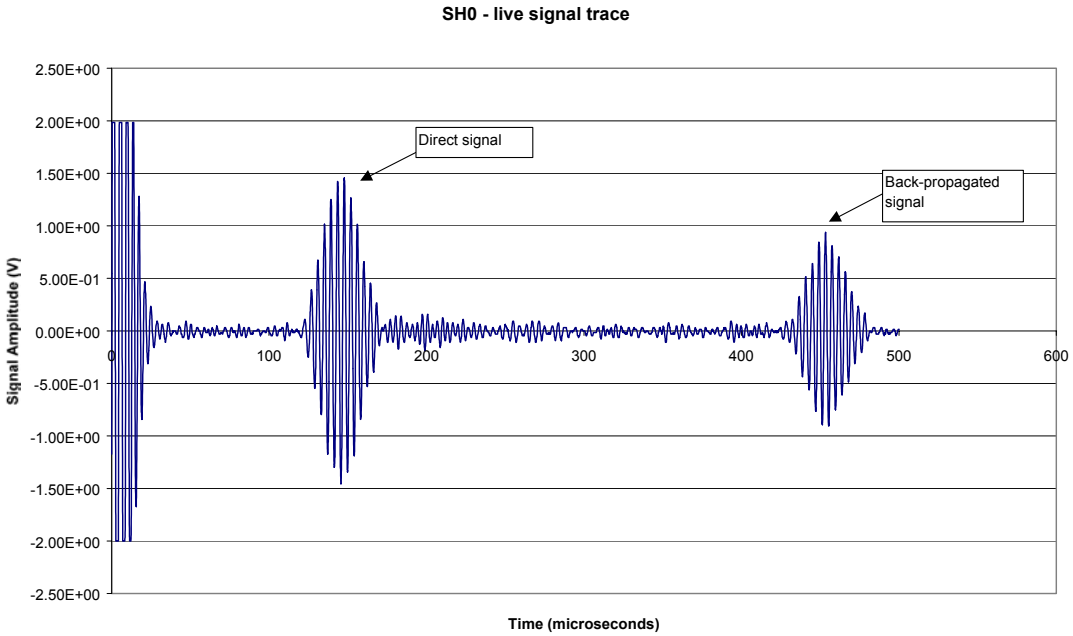

Figure 25 Example live trace of the received signal from an SH0 toneburst (using most recent SH0 'mouse' set-up

Reflection and Transmission From Man-made Cracks

The reflection/transmission crack interaction results for the 8.4 mm thick flat plate are summarised in 26 and 27, in which reflection coefficients are red, and transmission are blue. The modelled results are presented by dashed lines, while the interpolated, measured curves are solid.

For both SV1 (at 3.9 MH-mm) and SH0 at (2.1 MH-mm), the modelled and measured coefficients exhibit similar trends versus crack depth and generally compare well up to about 40% crack depth. Also, there are significant effects from the cracks. For example, a crack depth of 20% has a 40% and 25% reflection for SV1 and SH0, respectively. This is well above the noise level and easily detectable. This gives a degree of confidence that guided waves may be used to both detect and size SCC defects.

Note that the SV1 curves indicate a higher sensitivity for shallow crack depths than deeper ones. This is because the SV1 reflection and transmission curves flatten above ~ 25% crack depth. For example, for a crack depth from 10% to 20% the SV1 reflection coefficient changes by .19, but from a depth varying from 30% to 40%, the SV1 reflection coefficient changes by only .10.

SH0 has a more uniform sensitivity to crack depth than SV1. For example, for crack depths from 10% to 20% and from 30% to 40% the SH0 reflection coefficient changes by .13. For shallow cracks this is less than that of SV1, so that it would be less useful in defining shallow cracks than SV1. However, for crack depths from 30% to 40%, the SH0 coefficients show greater sensitivity to cracks, and so SH0 would be more useful in defining deeper cracks than SV1.

Unfortunately, the measured SH0 coefficients flatten above 40% depth, and we could not investigate above 50%. Coefficients for cracks deeper than 50% need to be evaluated in the future.

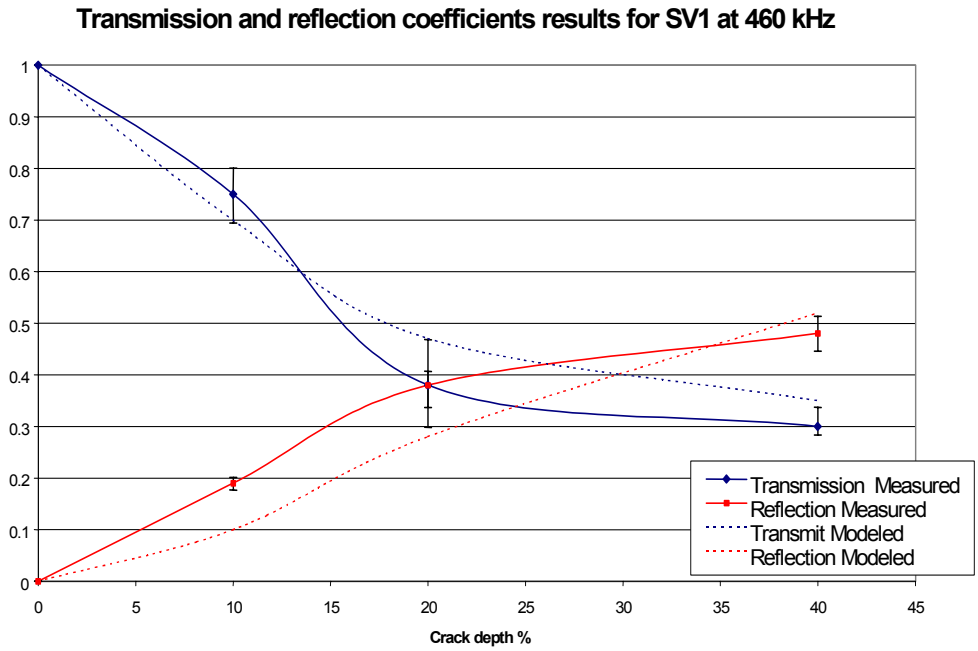

Figure 26 The measured and modelled reflection and transmission coefficients for interaction of the SV1 mode at 3.9 MHz-mm with a cracks of varying depth.

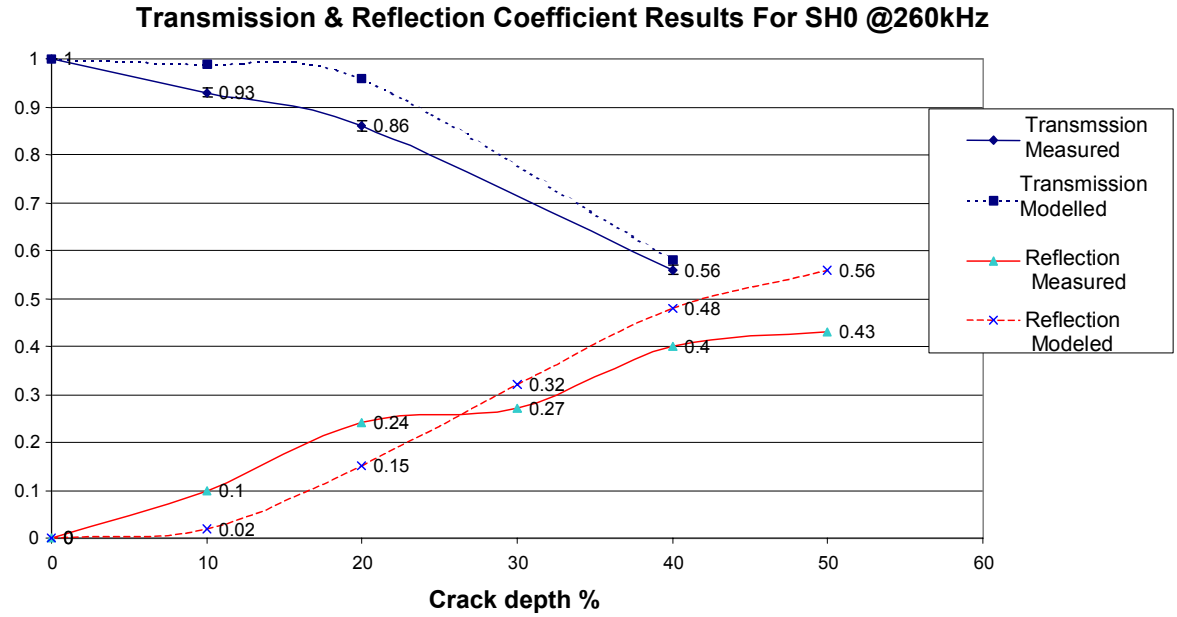

Figure 27 The measured and predicted reflection and transmission coefficients for interaction of the SH0 mode at 2.1 MHz-mm with cracks of varying depth.

Beam Width

The results for the two beam width measurements, corresponding to the geometries of Figures 9 and 10 , are shown in Figure 28 and 29. They indicate that for this particular geometry of EMAT coil, very little beam divergence occurs up to propagation distances exceeding 500 mm. Figure 29 indicates a regular shaped angular response with no side lobes at 90 degrees to create confusing artifacts.

Moreover, if we take the beam width to be the within points where the amplitude is decreased by .3 from the peak at the beam center, we can see from Figure 28 that the beam width is +- 4 cm or 80 mm wide. This is about the width (i.e. perpendicular to the propagation direction or the EMAT periodic pattern) of the EMAT ML coil. For circumferential waves the beam width is basically the axial (i.e. cross beam) resolution for simple processing of transmitted and reflected signal. In this case the resolution is 80 mm, which is probably tolerable based on discussions with some customers.

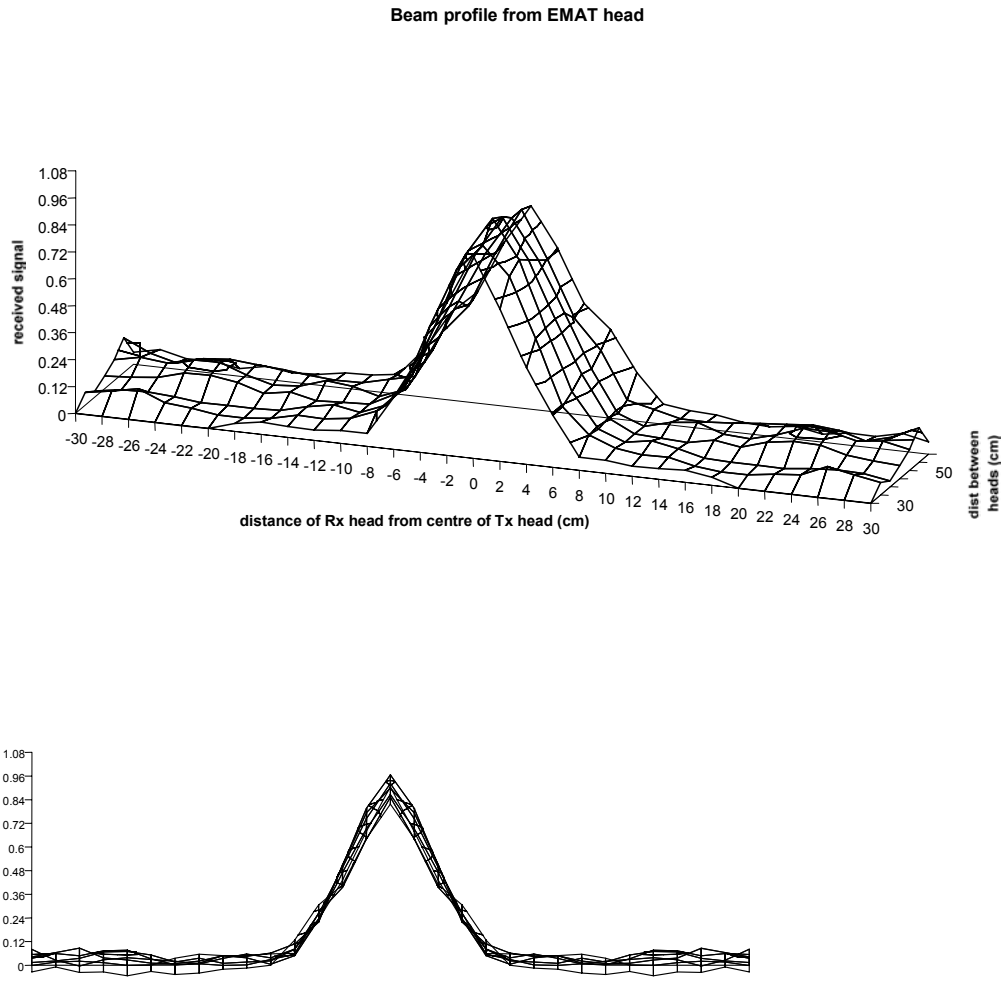

Figure 28 Beam profile of the SV1 EMAT transmit coil (80mm wide)

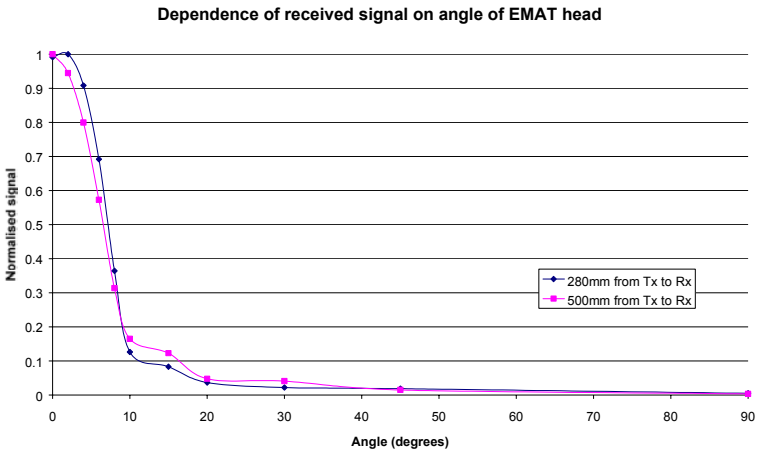

Figure 29 Angular dependency of SV1 mode.

Effect of Bias Field

The results using a bias field sweep through both positive and negative field values are given for the SV1 mode (3.91 MHz-mm) in Figures 30 and 31. These plot received signal amplitude (vertical axis) versus bias magnetic current, which is effectively the magnetic bias field. Note that the bias current from one transducer was swept while the other was held at a fixed value. Note also that portions of sweeps, referred to here as "quadrants" that have different histories (i.e. current increasing, decreasing, or at a later time) are shown in different colors.

For the SH0 mode (2.14 MHz-mm), the same experiment for the transmitter bias field dependency is shown in Figure 32. For the receiver, bias field dependency results are displayed for the positive quadrant only, in Figure 33, and higher currents were used to take the steel to full saturation.

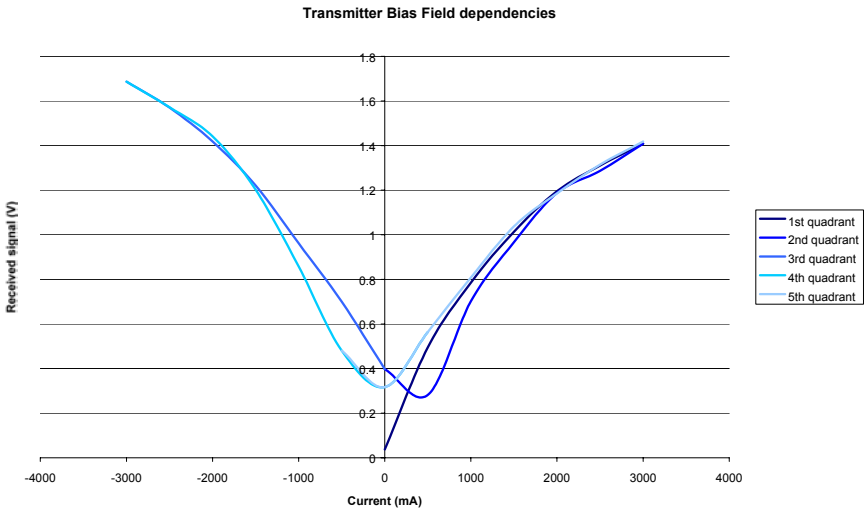

Figure 30 Dependency of the signal amplitude for the SV1 mode on the bias field of the transmit EMAT coil

These figures indicate that for transmitter and receiver EMAT coils and for either SV1 and SH0 modes 1) signal level is proportional to bias level and 2) the maximum signal occurs for magnetic saturation. Also, because saturation was not truly reached, there may be some room for further increases in signal amplitudes and SNRs above those obtained in the flat plate.

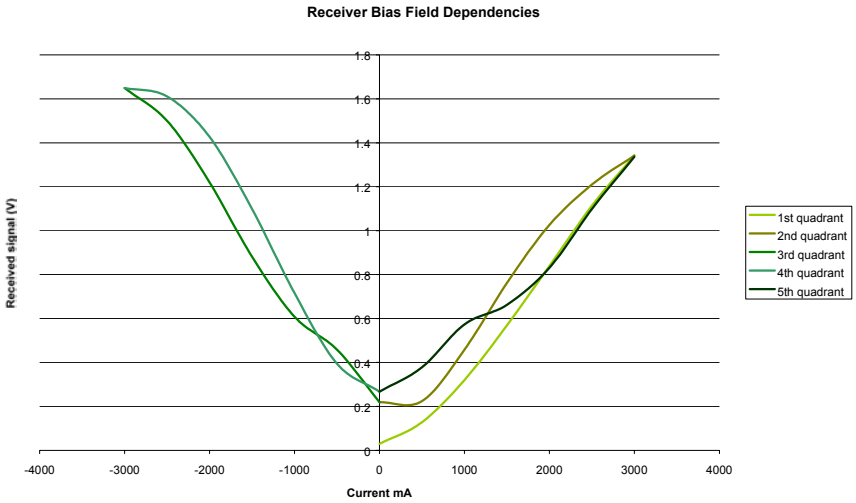

Figure 31 Dependency of the signal amplitude for the SV1 mode on the bias field of the receiver EMAT coil.

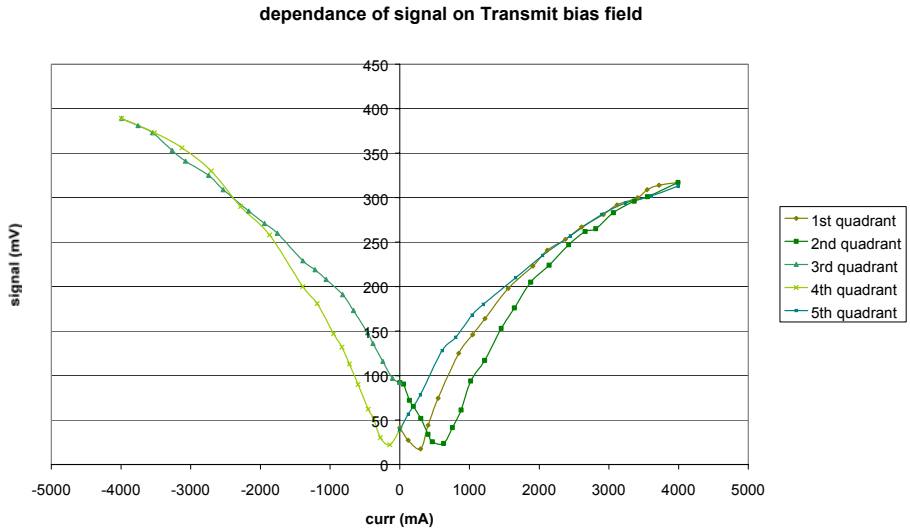

Figure 32 Dependency of the signal amplitude for the SH0 mode on the bias field of the transmitterer EMAT coil.

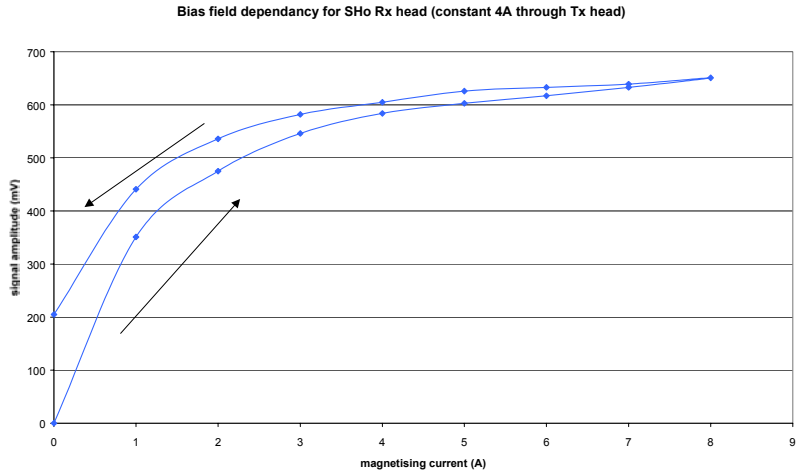

Figure 33 Dependency of the signal amplitude for the SH0 mode on the bias field of the receiver EMAT coil at high bias currents.

The SV1 and SH0 signal level dependencies on magnetic bias were investigated again in a 24 inch diameter full pipe as a check against the previous results in a plate or pipe sections. This was done with the transducers separated as if they were in a useful configuration. The reason for this check was that the transducer bias magnets would be close enough to interact in the closed pipe. For these tests the bias level on one type transducer was swept while the other bias for the other was held at saturation. The conclusion was the same as on the plate - that the best signal level for either mode was obtained with simultaneous magnetic saturation for both the transmitter and receiver.

Sensitivity to standoff and tilt

The effect of stand-off is shown in Figure 34: for the receiver in blue and the transmitter in green. A value of 1 represents a normalized amplitude with minimal standoff. These measured results fit the predicted dependence for a meander line (ML) coil relatively well [8]. For a ML coil, the signal amplitude is expected to follow exp(- c G/D), where G is the coil standoff from the surface, D is the interline spacing for the meander coil, and c is a positive constant. A good fit to the data was obtained for $y = 1.08e^{-0.67x}$. Thus, standoff sensitivity is as expected and decays exponentially with the ratio of standoff to wavelength.

D is half the wavelength for the mode being excited or received if the EMAT is chosen properly. Thus, amplitude versus standoff should depend on wavelength. By this reasoning the results for the SH0 (at 260 KHz) EMAT coil will be identical since its modal wavelength is very similar and the coil geometries are the same. Also shorter wavelengths will have smaller D, and hence larger G/D. Because of this they will allow less standoff in absolute terms and be more sensitive to standoff.

Note that we believe we can tolerate an amplitude reduction to .3. This corresponds to a standoff of up to 2 mm for SV1 (470 kHz) and SH0 (160 kHz).

The dependence of the received signal amplitude on tilt angle is shown in Figure 35. Front to back tilt, is shown is pink/purple, and sideways is shown in blue. It can be seen that for this coil design the signal is most sensitive to 'sideways' tilt (with respect to the propagation direction) as compared to 'front-to-back' tilt. Clearly these results will impact upon the mechanical design of

the sensor head if this coil (or variant of it) is used in the final system. Note that on an ILI pig, front-back is really circumferential and sideways is really axial for a magnetostrictive EMAT.

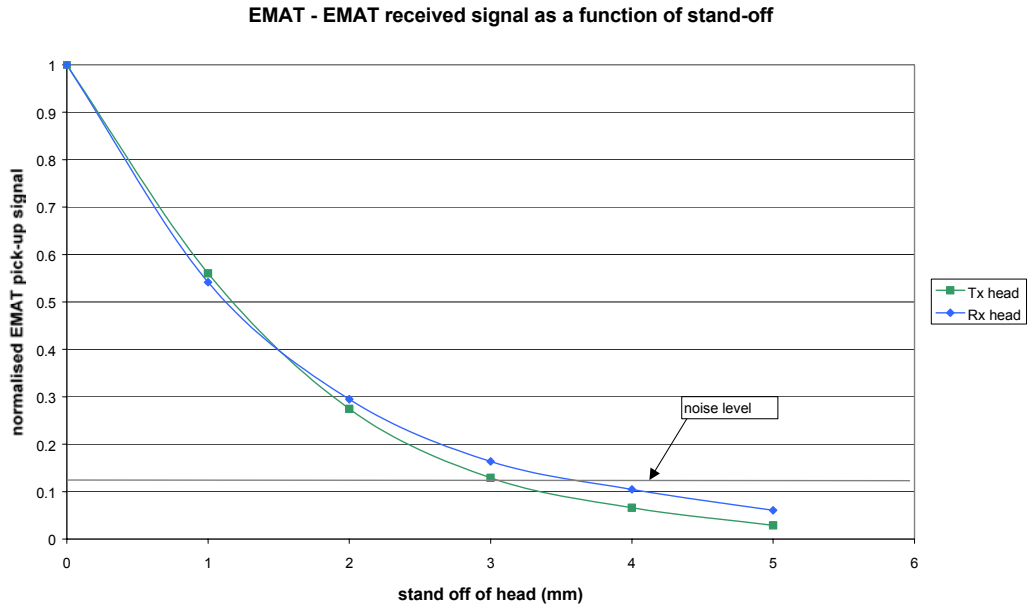

Figure 34 Effect of stand-off on the signal amplitude for EMAT-to-EMAT; SV1 coil. (Note that standoff is actually .1 mm larger marked. Thus, 0 standoff is actually .1 mm)

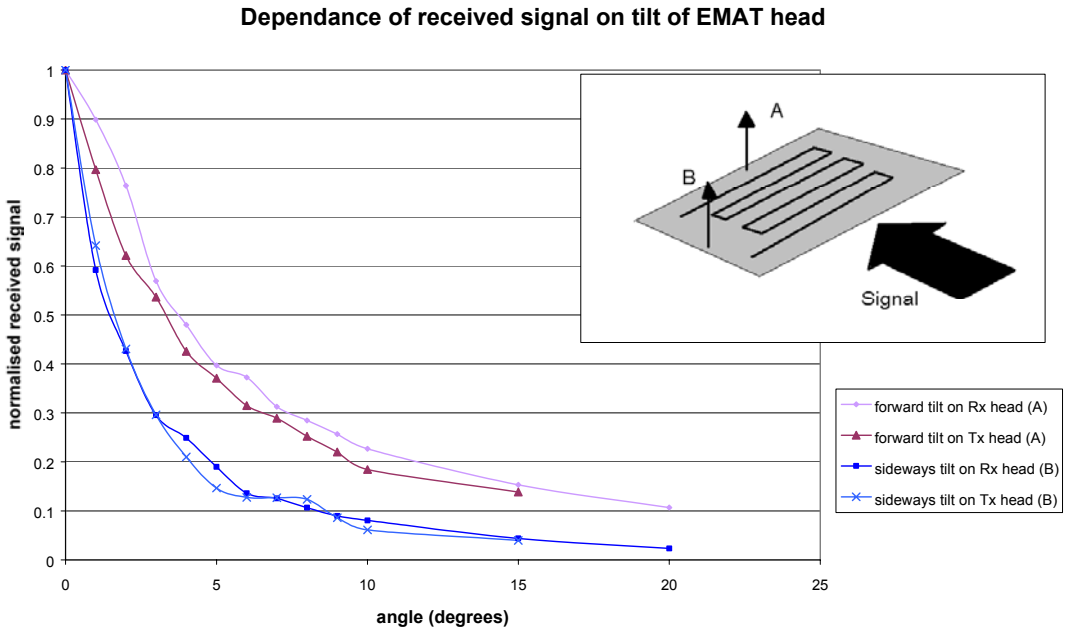

Figure 35 Effect of tilt on the signal amplitude for EMAT-to-EMAT; SV1 coil.

Note that the amplitude variation for standoff and tilt in Figures 34 and 35 are nearly identical for transmitter or receiver. It is expected because the transmitter and receiver EMATs should be reciprocal and they have the same geometry and biasing.

Detectability of SCC on a sample section

The length and depth of the defects in the sample of Figure 17, as indicated in supporting documentation provided by the supplier, are summarised in Table 2. Some preliminary work was done using angle shear bulk acoustic waves in order to facilitate the interpretation of the signals obtained from interaction of the EMAT guided waves with the SCC sites. These images, which show the defects rotated by 90 degrees clockwise to the plan, are shown in Figure 36.

Table 2 Pipe Section Defect Qualification (Lengths and Depths)

Pipe Sample #1

Defect ID	Approximate length (mm)	Approximate depth (%)
#106	80	20-25
#93	70	15-20
#90	20	7-10
#94	30	7-10

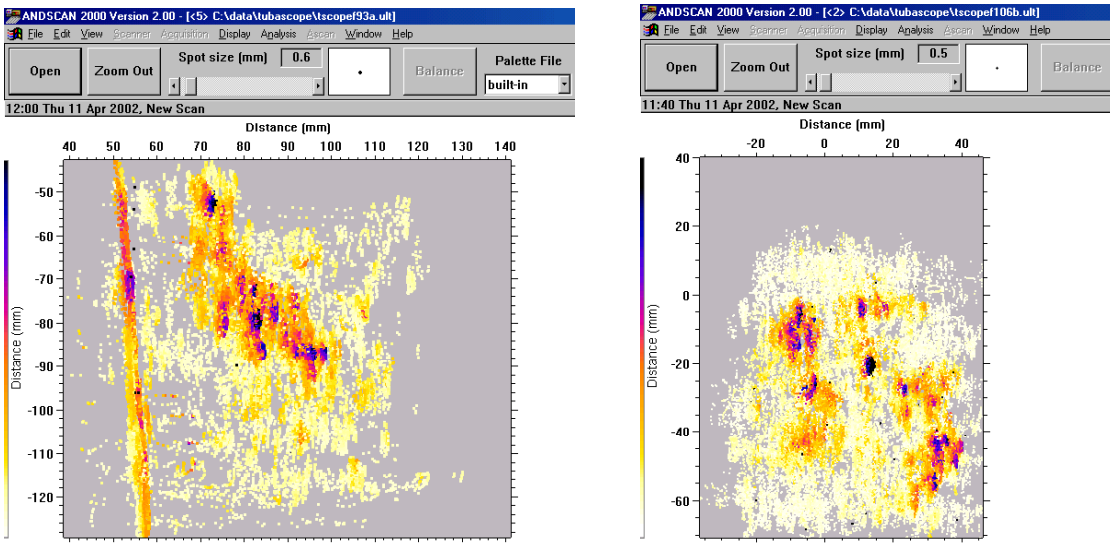

Defect # 93 Defect # 106

Figure 36 Analysis of defects #93 and #106 by bulk angled shear wave ultrasonic technique.

SV1 Transmission Results

According to the set up (Figure 13), the main interaction of the guided wave modes is expected to occur with defect #93 in the middle (~ 150 mm). The variation in the signal amplitude, normalised against the maximum received signal, of the directly received SV1 mode as the EMAT heads are scanned along the specimen is shown in Figure 37.

Although these results are far from conclusive, it can be seen that the maximum reduction in transmitted signal occurs between 110 mm and 180 mm along the specimen, which approximately corresponds to the position of the SCC defect #93.

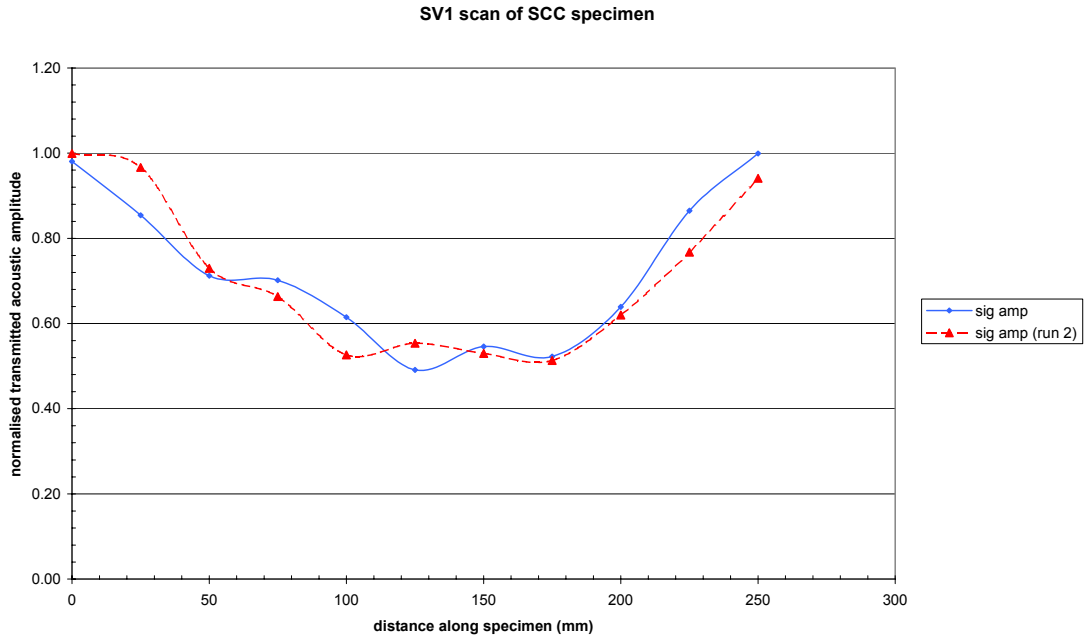

Figure 37 Variation in the amplitude of the direct transmitted SV1 signal as the EMAT heads are scanned along the SCC specimen.

SH0 Transmission Results

For SH0 the variation in direct signal amplitude as the heads are scanned along the specimen is shown in Figure 38. These results are less positive than those obtained for SV1. To some extent these results are expected because defect #93 is relatively shallow (max. 15-20% depth, average depth across transducer beam is much lower, and because SH0 is not sensitive to shallow cracks. The results were further complicated by the drift of signal amplitude with distance along the specimen, and the presence of other defects in the specimen.

SV1 and SH0 Reflection Results

Any analysis of this data proved to be extremely difficult and somewhat speculative due to reflections from the edges, and the fact that the transmitter passed over a defect. Because of this and because we had seen enough SCC interaction for transmission measurements, work with SCC pipe sections was stopped in favor of work in full circumference pipes with a mouse.

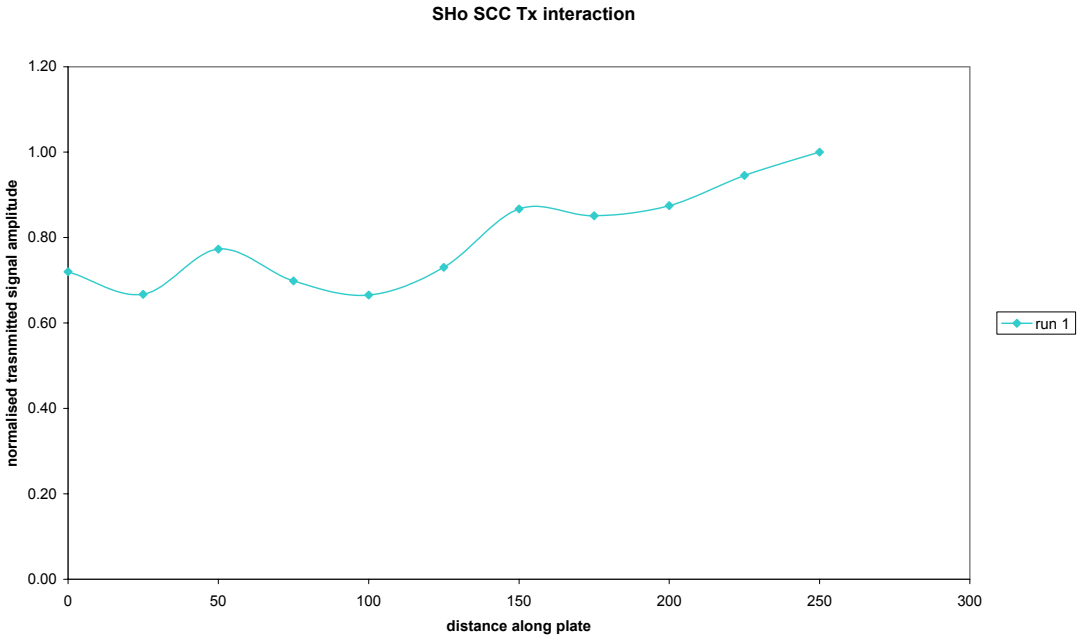

Figure 38 Variation in the amplitude of the direct transmitted SH0 signal as the EMAT heads are scanned along the SCC specimen.

Lab Mouse Preliminary Results

The geometry of the pipe and defects is shown in figure 39. The SCC sites were somewhat aligned. Some of the sites consisted of small cracks that appeared to be linked at the surface, others appeared to be continuous long cracks.

To better understand the nature of the defects and in order to provide some degree of defect sizing, the defects were characterised using angle shear wave ultrasonic techniques. The method is shown schematically in Figure 40. Top-down photos and ultrasonic images are juxtaposed and displayed in figures 41 and 42, along with an inch scale. In them, the color contours only indicate the amplitude of the signal return and do not indicate the absolute depth of the defects. From these images, all the cracks are narrow with a high length to width aspect ratio. Some like, P2-1, are continuous at the surface, as shown by the photo, and give strong ultrasonic reflections. Others like P2-7 are discontinuous at the surface and give weak ultrasonic reflections.

The angled shear technique, especially for crack depth determination, is still under development and a number of assumptions are made, such as the crack is vertical (normal to the surface), which are not necessarily met. The depth profiles have been determined at the center of defects P2-1 and P2-4, and are given in 43. Clearly, defect P2-1 is deeper than defect P2-4. The depth of defect P2-1 can be estimated to be approximately 15-20% through thickness.

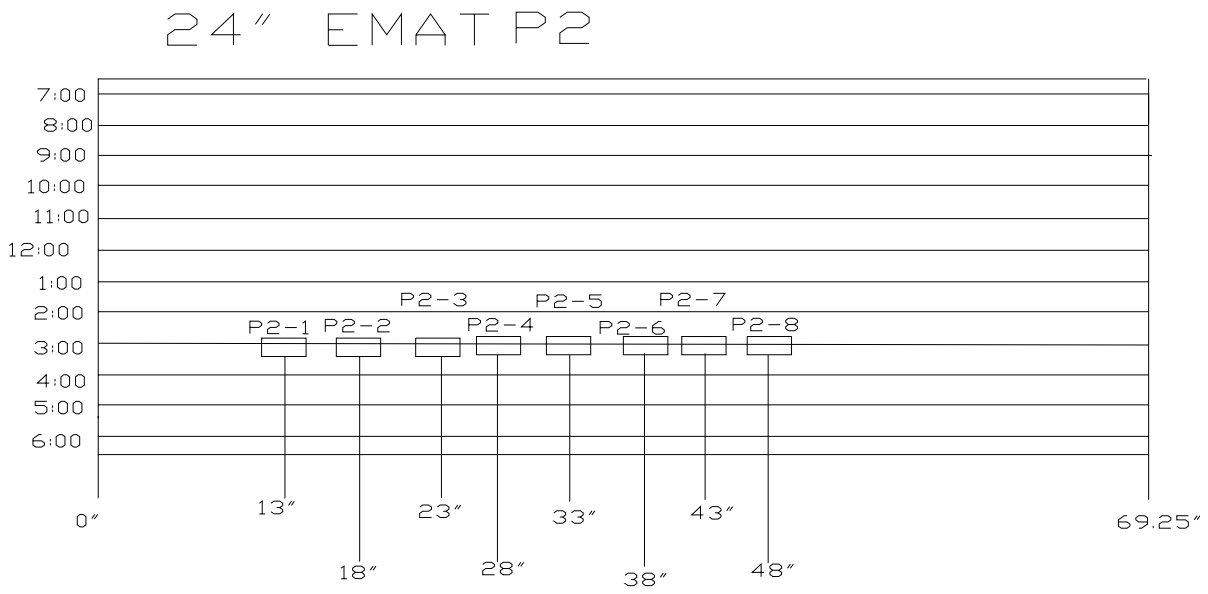

Figure 39 Positions of the defects in pipe sample P2.

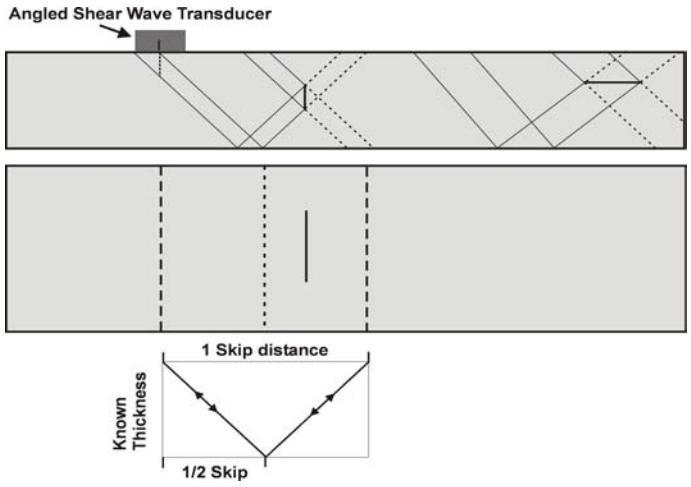

Figure 40 Schematic of the angled shear wave technique used to characterise the P2 defects.

Defect P2-1

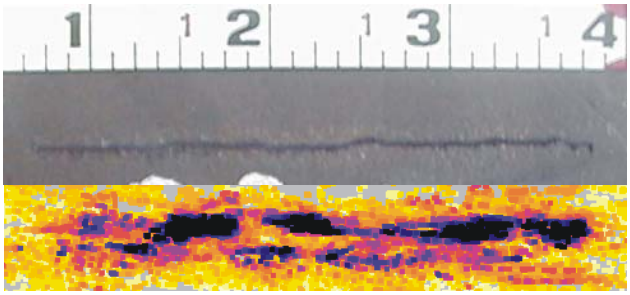

Photo

Ultrasonic

Defect P2-2

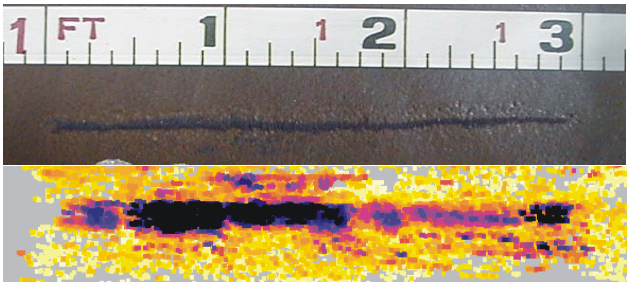

Photo

Ultrasonic

Figure 41 Top-down images of the defects P2-1 to P2-4 as characterised by the bulk angled shear wave technique.

Defect P2-5

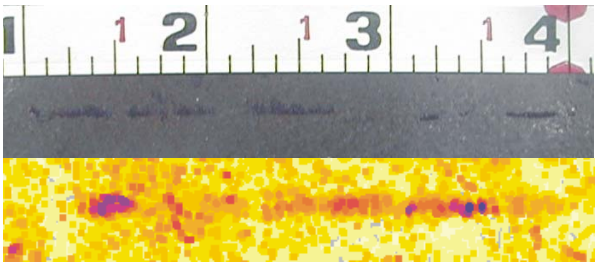

Photo

Ultrasonic

Defect P2-7

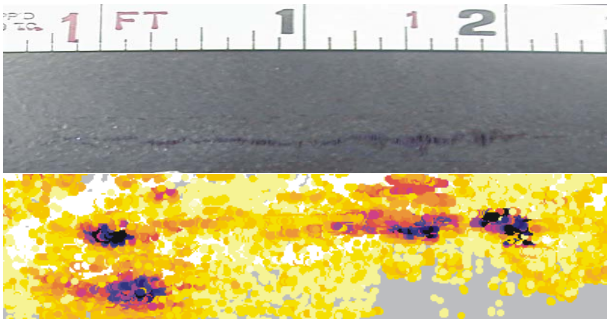

Photo

Ultrasonic

Figure 42 Top-down images of the defects P2-5 and P2-7 as characterised by the bulk angled shear wave technique.

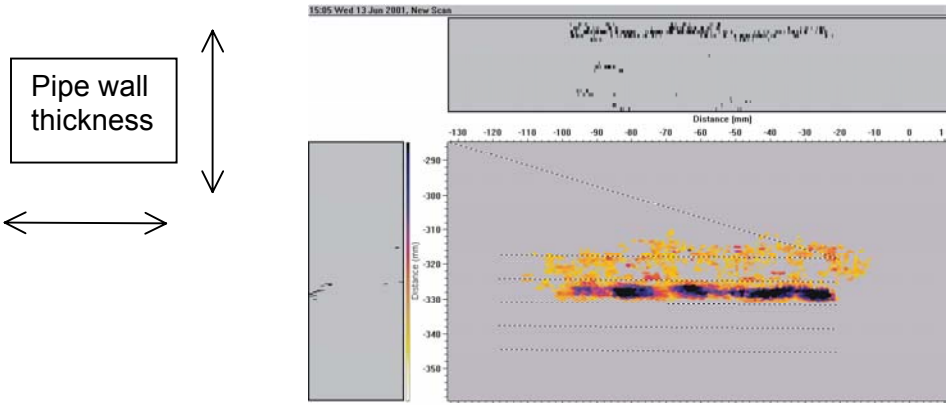

(a) P2-1 defect

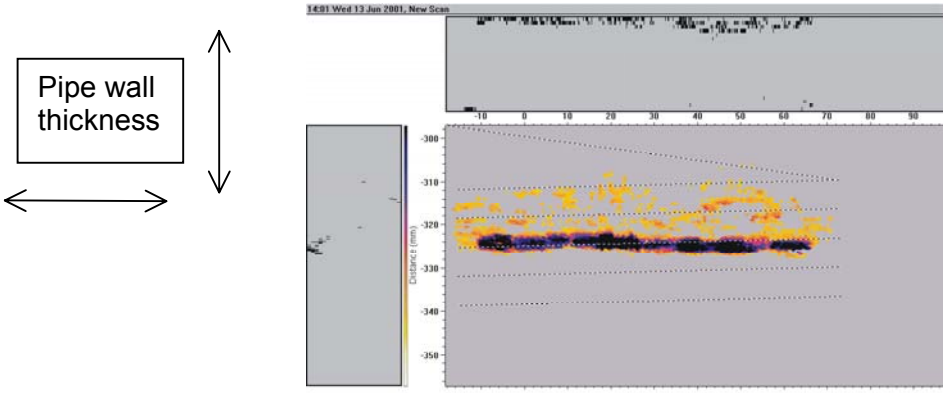

(b) P2-4 defect

Figure 43 Depth profile at the centre of the defects P2-1 and P2-4 as characterised by the bulk angled shear wave technique.

Initial Pipe Scan Results with the Test Mouse

SV1

Figure 44 shows an example trace from a spot without defects at the far end of the pipe. The trace clearly shows the following arrivals (in order): the firing breakthrough, the direct arrival (travelling counter clockwise 90 degrees), a small A1 mode arrival (travelling counter clockwise 90 degrees), the back-propagated arrival (travelling clockwise 270 degrees), a second direct arrival (travelling counter clockwise 450 degrees). The A1 arrival is a parasitic excited because its wavelength is similar to that of the desired SV1 mode. The A1 amplitude is about 1/20 that of the direct amplitude, which indicates good modal purity.

Figure 45 shows a trace taken at the axial position of P2-3 that contains a reflected signal from the line of defects in addition to the arrivals noted for the previous trace. The time after the direct signal at which a signal from the defects should occur can be calculated as follows.

Distance between Rx head and line of defects = 265 mm

Group velocity of SV1 mode = 4949 m/s

Therefore: Time between direct signal and reflected signal = 0.265*2/4949 = 107 microseconds.

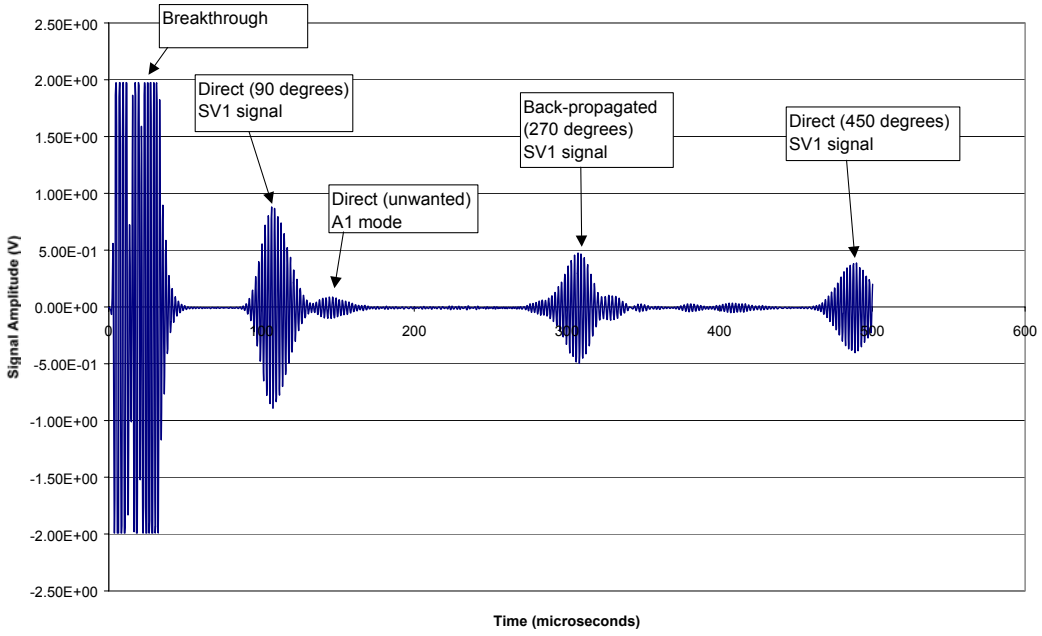

Figure 44 Example trace from the SV1 mouse carriage at a position 1180 mm along pipe (no defects present).

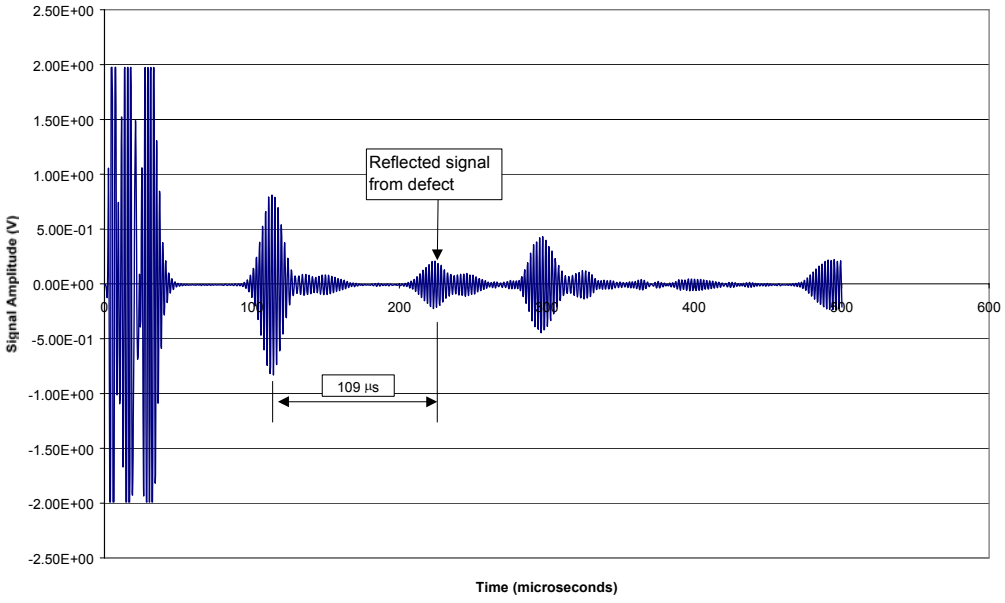

Figure 45 Example trace from the SV1 mouse carriage at a position 555 mm along pipe (defect present).

This corresponds with the time difference between the direct and reflected signal confirming it is a reflection from the line of defects. The small signal following the reflected signal can be attributed to reflection of the A1 mode and/or reflection of a mode-converted mode.

SH0

Figure 46 shows an example trace from a defectless position at the far end of the pipe. The arrival content is similar to the SV1 defectless trace. However, there are a few differences: First, the arrival times are different because the SH0 mode group velocity speed is slower. The round trip counter clockwise is absent because it is too late to be included. The mode of the small amplitude signal just after the SH0 direct arrival is unknown. However, its amplitude is about 1/20 that of the direct, which shows that the direct has good modal purity.

Figure 47 shows an example trace with a reflected signal from the line of defects at P2-1. The time after the direct signal at which a signal from the defects should occur can be calculated as follows.

Distance between Rx head and line of defects = 295 mm

Group velocity of SH0 mode = 3260 m/s

Therefore: Time between direct signal and reflected signal = 0.295*2/3260 = 180 microseconds.

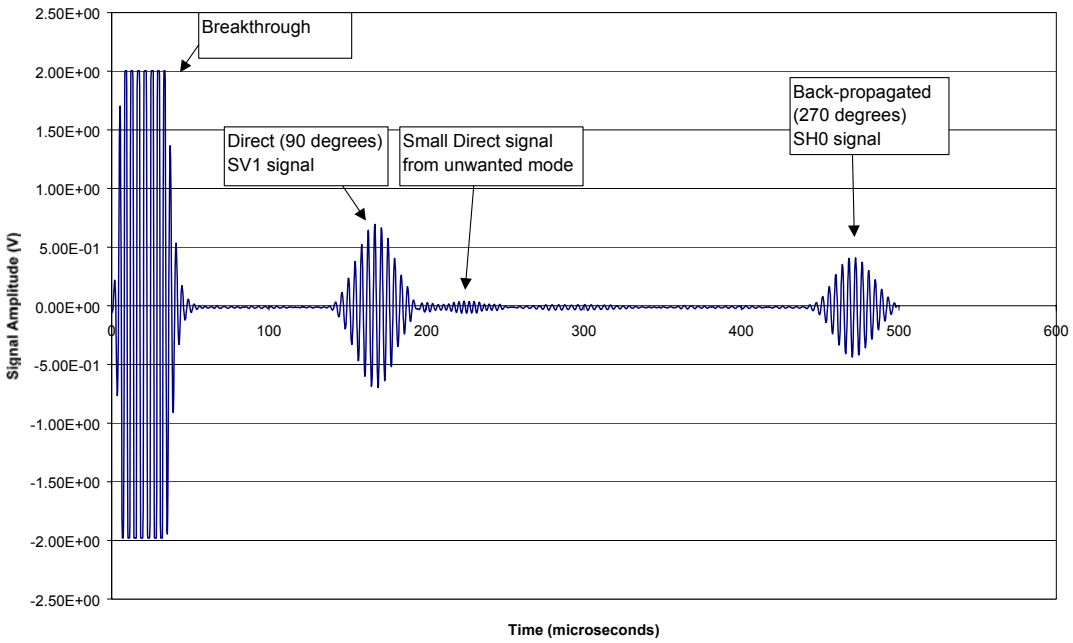

Figure 46 Example trace from the SH0 mouse carriage (set-up #1) at a position 1372 mm along pipe (no defects present).

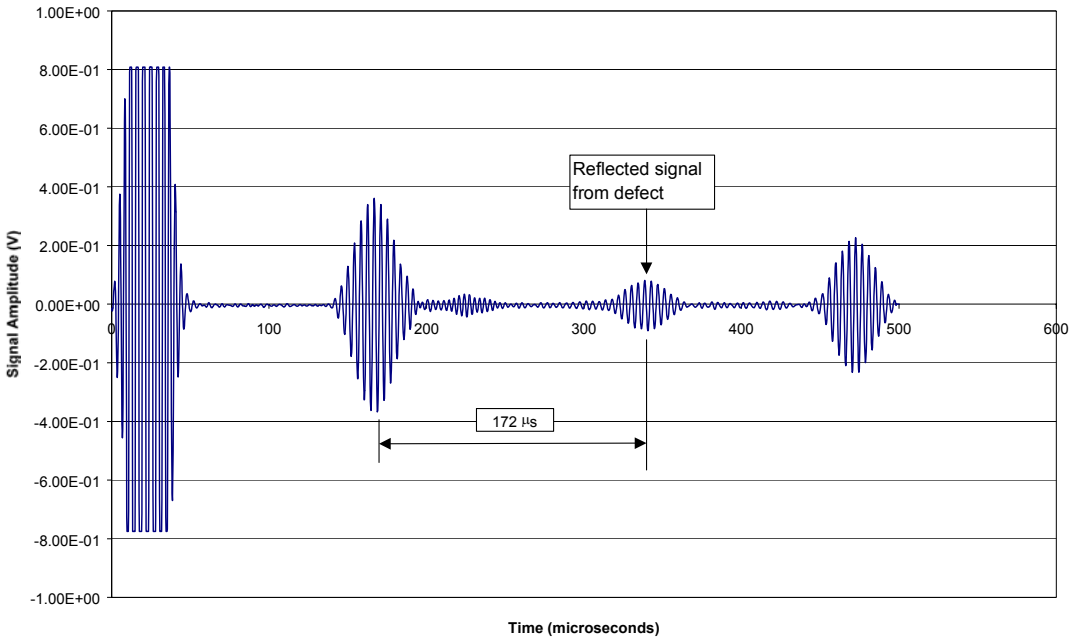

Figure 47 Example trace from the SH0 mouse carriage (set-up #1) at a position 322 mm along pipe (defect present).

This corresponds approximately to the time difference between the direct and reflected signal confirming it is a reflection from the line of defects.

Further Transducer Improvements For the Mouse & ILI Considerations

Some work was done to arrive at a high level design of a practical prototype EMAT sensor and measurement system that could then be applied first to the test mouse and later to a real ILI tool. In this work we investigated deployment/running issues: such as coil improvements, magnetic configurations, power requirements, and specifications for the electronics and data capture. From the plate investigations, we decided to consider the pitch-catch configuration, only. This is because applications to pitch-multiple-catch could be determined from simple pitch-catch and because pulse echo would be too complicated or noisy to be practical

EMAT Coil improvements

Double-layer coils were fabricated for the transmit head. The consisted of two coils, with the same widths, periods, and other parameters, stacked on top of each other and connected in series. These improved the SNR. Although the overall impedance of the coil increased, a less critical matching network more than doubled the current, so a larger dynamic field was applied compared to a single layer coil. Slightly higher SNR was achieved again by the use of three and four layer coils, but in considering ease of manufacture, double-layer coils are presently best.

Tool and Test Mouse Acquisition Specifications

The specifications for data acquisition requirements are based on the specs of the Le Croy 9354A digital oscilloscope used to capture the data in the laboratory-based flat plate and mouse experiments.

Table 3 Data Acquisition Specs For an EMAT System In 30" Pipe

Parameter	Value	Remarks
Digitizer Voltage Resolution	8 to 12 bits	At least
Digitizer Sample Rate	5 MHz	
Digitized Interval (time)	750 us	Per receiver (30" Pipe)
' ' (samples)	3750 samples	For 360 degree coverage
Transmitter Drive	5 cycle tone burst	
Transmitter Drive sample rate	5 MHz	
Firing Rate	500 Hz	Per transmitter head
Transmitter Drive Frequencies	220 kHz, 460 kHz	
Transmitter Instant. Power	140 Watts	Minimum
Transmitter Average Power	1 Watt	Minimum

The sample rate above provides enough data points to accurately determine the peak magnitude digitally and enough data for performing any further detailed analysis (e.g. FFT). The data interval provides enough time for SH0 and SV1 modes (at the chosen frequencies) to travel fully around the pipe and for a receiver to look ahead half way around the pipe. To inspect the whole circumference would require at least two receivers. If more receivers and transmitters are used, the digitization interval and the number of samples can be reduced.

The firing rate can be increased if the digitized interval is shortened to much less than 750 us. This would is reasonable with more receivers and transmitters arrayed around the circumference of the pipe.

Transmitter Power requirements

The instantaneous power consumption of the double-layer transmit coils is approximately 92 Watts for the SV1 mode. This is based on a coil resistance of 1.35 ohms (at 470 kHz) and a measured peak current of ~8 Amps flowing through the coil. The transmit head power amp and supply must have sufficient reserve to provide the instantaneous power. The instantaneous power consumption for double-layer SH0 transmit head is ~140 W based on a coil resistance of 0.9 ohms (at 260 kHz) and a measured peak current of 12.4 Amps. This instantaneous power will increase *pro rata* with increased drive current if (a) a higher SNR is required or (b) stand-off of the coil from the pipe surface is increased.

The batteries only must supply the average power, which takes into account the pulse duration and firing rate (i.e. the duty cycle of the instantaneous power). For SV1 at 470 kHz, based on a pulse duration of 5 cycles at 470 kHz (10 us) and a firing rate of 500 Hz, the average power requirement of a single transmitter EMAT head is approximately .5 Watt [4] . Note that the firing rate of 500 Hz (equates to a reading every 0.2“ for a tool travelling at 5.6 mph). The average power per transmitter head for the SH0 mode is ~1 Watts because the higher instantaneous power and lower frequency (longer duration).

The power requirements for the Receiver EMAT head are dependent on the power requirements of the signal amplifier stage. For the pre-amplifier used in this work the total power consumption was approximately 0.11 Watts, assuming the preamp is "on" continuously. Compared to transmitters, receivers can almost be neglected. Even for multiple transmitters

[4] Not accounting for the power consumption of power amplifier and signal generator electronics.

and receivers, these power requirements look reasonable compared to a 30" ILI high resolution magnetic flux leakage tool, which could be drawing 15 to 20 Watts for its Hall sensors

Permanent Magnet Bias Configurations

For the axial magnetic bias for SH0, two basic configurations were considered. One is the classic brush design used in Tuboscope's MFL tool with brushes in contact with the pipe ID and covering 100% of the circumference. The other has a finite number of modules, referred to as sleds, around the circumference. Each module had pole faces with a fixed air gap between the pole faces and the pipe ID. The sled design has the advantages of gas bypass, having less magnetic material, less weight, and less friction. It has the disadvantage that is it more complicated to support and as new concept, requires engineering development.

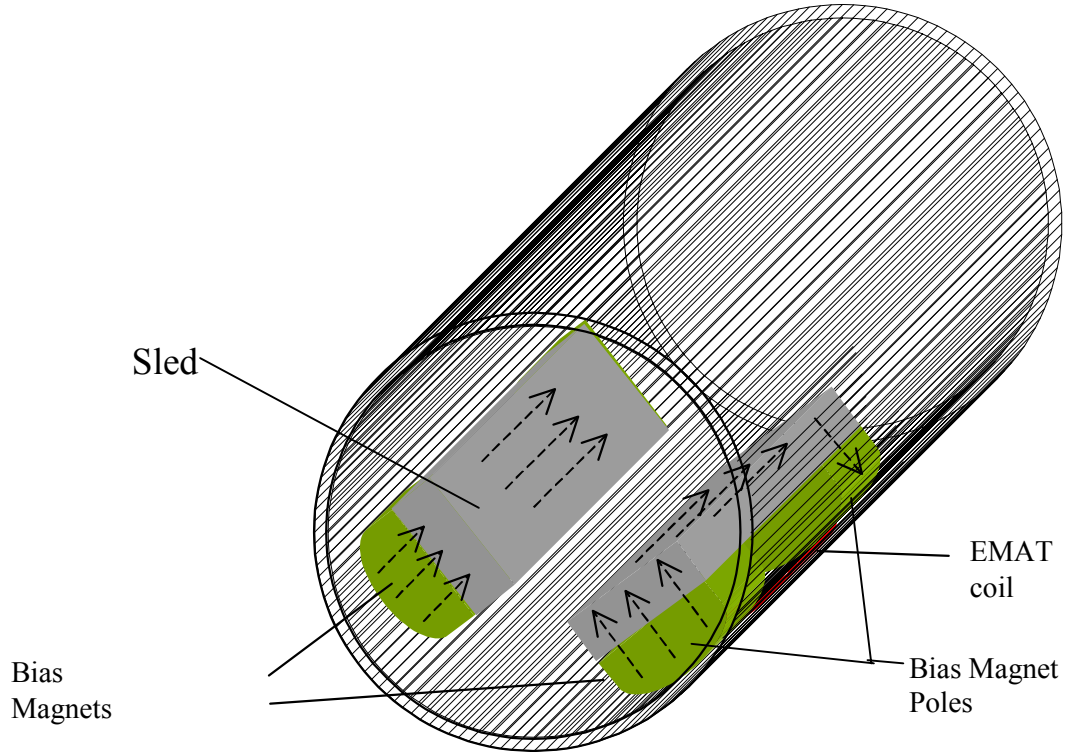

Figure 48 The design for a 30" sled-based axial magnetiser for SH0 .

A sled module would provide an excellent base for an EMAT ML coil and support electronics. An EMAT ML coil could be independently sprung in the gap between the poles of the sled, minimizing the inertia of the head, allowing it to rapidly move out of the way of obstructions, and thus, minimizing the possibility of impact damage.

Summary and Conclusions

This report describes progress, experiments, and results for a project to develop a pipeline in-line inspection tool that uses electromagnetic acoustic transducers (EMATs) to detect and grade stress corrosion cracking (SCC). The time period is from October 2001 through the end of January 2003. There is a brief introduction that gives background material about EMATs and relevant previous work for the Gas Technology Institute**.** This work left six choices for the acoustic modes and a choice between magnetostrictive or Lorentz type transducers for this project.

The experimental section then describes the lab systems, improvements to these systems, and setups and techniques to narrow the choices. Improvements, which involved transducer matching networks, better magnetic biasing, and lower noise electronics, led to improved signal to noise (SNR) levels and modal purity of waves launched and received by EMATs. The setups permitted transducer characterizations and interaction measurements in plates with man-made cracks, pipeline sections with SCC, and a full pipe with SCC. The latter were done with a moveable and compact EMAT setup, called a lab mouse, which is detailed. The mouse system will next be used for scans of the SCC pipe.

Next, the results section justifies the mode and transducer choices. These were for magnetostrictive EMATs and the use of EMAT launched modes: SH0 (at 2.1 MHz-mm) and SV1 (at 3.9 MHz-mm). The other modes had distinct problems such as, a very low SNR, too high a frequency, too high a theoretical attenuation, or poor spatial resolution. In general, some theoretic modal properties along with the experience of the improvements and measurement results impacted this choice, which met a major project goal. The main justifications were good SNRs, useful crack sensitivity, and practical implementation. However, both SH) and SV1 were evenly matched, so both were pursued. The advantages and disadvantages of both are in the Table 3.

Table 3: Comaprison of SH0 and SV1 Modes

Mode	SV1	SH0
Advantages		
	Modal puriiy	Modal purity
	Very High SNR	Moderate SNR
	Crack sensitivity shown	Crack sensitivity shown
	Crack senstivity aggreement with theory	Crack senstivity aggreement with theory
	Very low dispersion	No dispersion
	Good beam to 500 mm	Good beam to 500 mm
Disadvantages		
	Modest attenuation	Very low attenuation
	Possible interference from A1 mode	Possible interference from SH1 mode

In addtion to the above advantages, it seemed that both the modes were complimentary in grading cracks. SV1, being more sensitive to shallow cracks, could be used to differentiate and grade shallow cracks, while SH0, which is disproportionally sensitive to deep cracks, could be used to identify and grade deep ones.

As for the type of transduction, we decided on magnetostrictive. After achieving best magnetic biasing, similar SNRs were achieved for both magnetostrictive and Lorentz. However,

magnetostrictive allows the bias magnets to be separated from the EMAT coil. Thus, the light coil could be held near the pipe without a heavy load on it, and the bias magnets, surrounding the coil, could even provide some protection. This is a much more rugged situation than occurring for a Lorentz EMAT, which must have the bias magnet above the coil. Another advantage of the magnetostrictive is that the bias field required is in the plane of the pipe rather than perpendicular. A perpendicular field is difficult to set up over a large area, without some spreading to planarity.

The results section then gives details of measurements on these modes. The measurements consisted of signal to noise ratio, insertion loss, magnetic biasing sensitivities, crack reflection and transmission coefficients, beam width, standoff and tilt sensitivities. For most of the measurements the section presents useful parametric curves - for example, reflection coefficient versus crack depth. The section shows scan results for a pipe section having SCC and mouse waveforms from a full pipe in areas with and without a defect. In preparation for a full tool, this section also reviews further coil optimisation and implementation requirements. These involve transmitter and receiver power, acquisition parameters, and magnetic configurations. Further results are beyond the time period of the report.

From the measurements and mouse results a number of conclusions can be drawn for magnetostrictively generated SH0 (at 2.1 MHz-mm) and SV1 (at 3.9 MHz-mm), on which the report focused. These are given below:

Magentostrictive EMAT were built and operated successfully. SNRs of >100:1 and ~30:1 has been achieved for SV1 and SH0, respectively with a stand-off of ~.1mm, high bias field (magnetic saturation) conditions, and a peak drive current of ~10 A for the transmit EMAT coil using a double-layer coil in series.

Measurements of reflection and transmission coefficients on a flat plate showed useful sensitivity to cracks for both the SH0 and SV1 modes. Additionally, the measured coefficients agreed well with theoretic values computed by means of 2 D FEM simulations. SV1 is sensitive to shallow cracks, while SH0 is sensitive to deeper (>20% wall thickness) cracks.

Beam width measurements, measured on a plate, showed that good, non divergent beams could be launched over useful distances like about 500 mm. This was done for 80 by 60 cm EMAT that was 5 wavelengths long. In the non-divergent zone the width was about that of the EMAT coil. Measurements also indicated that the EMAT did not have sidelobes.

Standoff measurements indicated that standoff decreases amplitude exponentially with the ratio of standoff to wavelength. Thus, very short wavelengths (or high frequencies) are at a disadvantage. Measurements showed that the SH0 and SV1 could tolerate 1 to 2 mm of standoff. There was a similar tolerance for tilt.

Various lab results and checks on the group and phase velocities of launched waves confirmed the requirements for magnetic bias directions. For magnetostrictive EMATs launching waves circumferentially around the pipe these requirements are: SH0 requires an axial magnetic bias, but SV1 requires a circumferential bias. Both of these are in the plane of the pipe wall not perpendicular to the pipe wall.

Magnetic biasing investigations were carried out on a plate, sections of pipe, and in full pipe using electromagnets. The final results showed that for transmitter and receiver EMATs for both

SH0 and SV1, the highest SNRs would be obtained with the steel with as high a B field as possble. That is at staturation.

Reflection and treanmission measurements were made on 120 degree arc sections of dug pipe containing real SCC. This was done for both SH0 and SV1 modes. The transmission measurements showed some effect and correlation to angle block generated, bulk shear wave acoustic responses. Unfortunately, reflection results on theses sample were too complicated to interpret because of edge reflections due to limited plate size.

For a lab mouse two carriers (one for SH0 and one for SV1) were designed and built and deployed on real pipe with some SCC defects. Each mouse had a pitch-catch arrangement with electromagnets. The orientation of the bias magnet and the drive frequency determined if SH0 or SV1 was logged. These units can be pulled through the pipe to simulate logging. The mice and software have been run on a preliminary basis to work out bugs, prove reliability, and verify SNRs. Special software allows waveform files to be conveniently built up as the mouse is stepped in 1 cm increments, simulating a logging situation. These all worked well.

In anticipation of a full size tool, power requirements, acquisition, and magnetic configuration requirements were compiled based on lab and mouse experience. Although tranmitter peak power requirements are high, the average power at reasonable logging speeds is low enough to be feasible even if multiple transmitters are used. Digitization rates are high but achievable with today's chips at low power in a full sized tool. In sum, nothing seen so far is a large hurdle for a full sized tool.

First EMAT mouse results look good and justify complete scans of the SCC pipe. SNRs and modal purity are good for both modes. Arrivals can be easily discerned that travel 450 degrees around the pipe. Easily discernible reflections with appropriate arrival times indicate promising crack interactions. These justify pushing ahead with complete scans for SH0 and SV1 with the mouse. These will be described in the next major report.

References

1. T. A. Bubenik, D.R. Stephens, et al, *Stress Corrosion Cracks in Pipelines: Characteristics and Detection Considerations,* Gas Research Institute Topical Report (for GRI Contract 5093-220-2692), April 1995.

2. H. M. Frost, "Electromagnetic-Ultrasound Transducers: Principles, practice, and applications", *Physical Acoustics Vol.* XIV (Academic Press, 1979), pp 179-275..

3. B. W. Maxfield and C.M. Fortunko, *The Design and Use of Electromagnetic Acoustic Wave Transducers (EMATs)*, Materials Evaluation, 41, 1399-408, (1983).

4. L W. Schmerr, *Fundamentals of Ultrasonic NonDestructive Evaluation*, A Modelling Approach, Plenum, Press 1998.

5. J. L. Rose, *Ultrasonic Waves in Solid Media*, Cambridge University Press, 1999.

6. R. Bruce Thompson, *Generation of horizontally polarized shear waves in ferromagnetic materials using magnetostrictively coupled meander-coil electromagnetic transducers*, Applied Physics Letters Vol. 15, pp 175-177, January 1979.

7. Riichi Murayama, *Driving mechanism on magnetostrictive type electromagnetic acoustic transducer for symmetrical vertical-mode Lamb wave of shear horizontal-mode plate wave*, Ultrasonics Vol 34 ,1996, Elsevier Publishing, pp 729-736.

8. R. B. Thompson, "Measurements with EMAT Transducers", *Physical Acoustics* Vol. XIX, Academic Press, pp 164-200, 1990.

9. M. G. Silk and K. F. Bainton, *The propagation in metal tubing of ultrasonic wave modes equivalent to Lamb waves*, Ultrasonics, 1979: pp 11-19.

10. J. L. Rose and X. Zhao, *Anomaly Throughwall Depth Measurements With Shear Guided Waves*, Materials Evaluation, October 2001, pp 1234-1238.

11. J C Hamilton, *The Development of An EMAT Based In-Line Inspection System For the Detection of Stress Corrosion Cracks In Operating Pipelines*, Gas Research Institute Final Report (for Contract 5095-270-3286), April 2000.

12. J. Aron, J Gore, et al, *Advanced Electro Magnetic Acoustic Transducer (EMAT) Technology for Determining Stress Corrosion Cracking (SCC)*, Gas Research Institute Topical Report (for GRI Contract 6030), January 2002.